Triggering of Tremors and Slow Slip event in Guerrero (Mexico) by the 2010 Mw 8.8 Maule, Chile, Earthquake.

Dimitri Zigone[1*], Diane Rivet[1], Mathilde Radiguet[1], Michel Campillo[1], Christophe Voisin[1], Nathalie Cotte[1], Andrea Walpersdorf[1], Nikolai M. Shapiro[2], Glenn Cougoulat[1], Philippe Roux[1], Vladimir Kostoglodov[3], Allen Husker[3], Juan S. Payero[3].

[1] Institut des Sciences de la Terre, Université Joseph Fourier, CNRS, IRD, BP 53, 38041 Grenoble, France

[2] Institut de Physique du Globe de Paris, Sorbonne Paris Cité, CNRS (UMR7154), 1 rue Jussieu, 75238 Paris, cedex 5, France.

[3] Instituto de Geofísica, Universidad Nacional Autónoma de México, CU, Coyoacan, 04510 México, D.F., México.

* now at Department of Earth Sciences, University of Southern California, Los Angeles, CA, 90089-0740

Corresponding author: dimitri.zigone@ujf-grenoble.fr

Abstract

We investigate the triggering of seismic tremor and slow slip event in Guerrero (Mexico) by the February 27, 2010 Maule earthquake (Mw 8.8). Triggered tremors start with the arrival of S wave generated by the Maule earthquake, and keep occurring during the passing of ScS, SS, Love and Rayleigh waves. The Rayleigh wave dispersion curve footprints the high frequency energy envelope of the triggered tremor, indicating a strong modulation of the source of tremors by the passing surface wave. This correlation and modulation by the passing waves is progressively lost with time over a few hours. The tremor activity continues during the weeks/months after the earthquake. GPS time series suggest that the second sub-event of the 2009-2010 SSE in Guerrero is actually triggered by the Maule earthquake. The southward displacement of the GPS stations starts coincidently with the earthquake and tremors. The long duration of tremors indicate a continuing deformation process at depth, which we propose to be the second sub-event of the 2009-2010 SSE. We show a quasi-systematic correlation between surface displacement rate measured by GPS and tremor activity, suggesting that the NVT are controlled by the variations in the slip history of the SSE. This study shows that two types of tremors emerge: (1) Those directly triggered by the passing waves and (2) those triggered by the stress variations associated with slow slip. This indicates the prominent role of aseismic creep in the Mexican subduction zone response to a large teleseismic earthquake, possibly leading to large-scale stress redistribution.

1. Introduction

Since their discovery in California [*Linde et al.*, 1996], Japan [*Hirose et al.*, 1999] and Cascadia [*Dragert et al.*, 2001], slow slip events (SSE) have been observed in a large variety of subduction zones (Japan, Cascadia, Mexico, Costa Rica, New Zealand, Alaska, see [*Schwartz and Rokosky*, 2007] for a review). These SSEs are sometimes associated with strong activities of seismic tremors in the so-called Episodic Tremor and Slip (ETS) observed for the first time in Cascadia by [*Rogers and Dragert*, 2003]. With the improving of GPS measurements, correlations between tremor and SSEs have been established in Cascadia and southwest Japan and there may exist similar correlations in Alaska [*Ohta et al.*, 2006; *Peterson and Christensen*, 2009], and Costa Rica [*Brown et al.*, 2005; *Outerbridge et al.*, 2010]. This study focuses on the Guerrero gap, located along the Mexican subduction zone (Figure 1) where some of the largest SSE were observed [*Kostoglodov et al.*, 2003]. During the last decade, 4 SSE have been reported with a recurrence interval of about 4 years (1998, 2002, 2006 and 2009-2010) [*Cotte et al.*, 2009; *Walpersdorf et al.*, 2011]. They reach equivalent seismic moment up to Mw=7.6 with a southward surface displacement up to 5-6 cm. The 2009-2010 SSE appears more

complex than the previous SSE in the region [*Kostoglodov et al.*, 2003; *Radiguet et al.*, 2011; *Vergnolle et al.*, 2010]. The slip takes place on two different portions of the fault. The total duration of the SSE is about 14 months, which is much longer than the previous events in Guerrero (about 6 months).

These SSEs are accompanied by a strong but irregular tremor activity located in central and northern Guerrero [*Payero et al.*, 2008] where the subduction interface remains horizontal at 40 km depth [*Kim et al.*, 2010; *Kostoglodov et al.*, 1996; *Pardo and Suarez*, 1995; *Perez-Campos et al.*, 2008]. A recent study [*Kostoglodov et al.*, 2010] reveals that the NVT activity in Guerrero is not simply correlated with the SSE. Even if the slow-slip is accompanied by a large amount of tremors, significant tremor activity is also observed between slip events, composing the background tremor activity and located further north from the SSE region.

In this study we investigate the triggering of tremors and slip events in Mexico by the great 2010 Maule earthquake (Mw 8.8) that occurred on February 27, 2010 at 6:34:14 (UT) off the coast of Chile. Dynamic triggering of seismic tremors by distant earthquakes has been observed in several regions (e.g. Japan, California, Cascadia, Taiwan) in the past few years [*Ghosh et al.*, 2009b; *Miyazawa and Mori*, 2005; 2006; *Miyazawa and Brodsky*, 2008; *Peng and Chao*, 2008; *Peng et al.*, 2009; *Peng et al.*, 2008; *Rubinstein et al.*, 2007; *Rubinstein et al.*, 2009] during the passage of Love waves [*Peng and Chao*, 2008; *Rubinstein et al.*, 2007] or Rayleigh waves [*Miyazawa and Mori*, 2005; 2006]; exceptionally, the passage of P waves [*Ghosh et al.*, 2009b] or S waves [*Shelly et al.*, 2011] might trigger tremors too. Triggered tremors by regional earthquakes have also been reported in California [*Guilhem et al.*, 2010]. By contrast, there is only few evidence of triggered SSE by distant earthquakes. *Itaba and Ando*, [2011] and *Rubinstein et al.*, [2009] suggested that large ETS events, which persist for more than one week, are sometimes dynamically triggered in the Cascadia subduction zone. Recently *Itaba and Ando*, [2011] observed a small slow slip event (equivalent magnitude 5.3) associated to the Mw7.6 Tonga earthquake of March 2009.

2. Data

The 2010 Maule earthquake (Mw 8.8) was recorded by the broadband sensors of the Sismologico Servicio Nacional de Mexico (SSN) and the very broadband UNM (GEOSCOPE) station in Mexico City. In addition, several seismic mini-arrays (referred hereafter as G-GAP network) have been deployed in central Guerrero since 2009 to study the tremor activity previously observed in that region [*Husker et al.*, 2012; *Kostoglodov et al.*, 2010; *Payero et al.*, 2008]. Each mini-array is composed of one broadband sensor (CMG40-60s by Guralp) in the center surrounded by 6 1s period sensors for a total

aperture of about 150 meters per array (Figure S1). To study the SSE, we use 5 GPS stations located in Guerrero along a profile from Mexico City to Acapulco (Figure 1). Tremors are identified in the 2-8 Hz frequency band as bursts of non-impulsive seismic energy. These bursts are coherent among 12 stations used in this study (see Figure 2 for the seismograms and Figure S2 in supplementary materials for a map of all 30 stations). The station UNM is used as a reference because it is equipped with a STS1 seismometer and it is located far away from the tremor zone.

3. Triggering and Modulation of Tremor Activity by the Mw 8.8 Chile earthquake

3.1 Immediate tremor triggering

We first analyze a limited time window corresponding to the passing of seismic waves from the Maule earthquake. Figure 3A shows a comparison of band-pass (2-8Hz) filtered record at ATLI mini-array and the seismograms recorded by the broadband UNM station in Mexico City on the transverse (green trace) and vertical (blue trace) components. Knowing the difference of 91 km in epicentral distance between the two stations, the time shift of the traces between the two records is 21 seconds, based on a 4.4 km/s Love wave phase velocity. We observe individual triggered bursts of 60 to 90 seconds duration associated with S, ScS and SS phases (arrival time 11 minutes, 12min20s and 16min10s respectively). The energy burst associated with the P wave arrival is not a tremor but the high-frequency energy associated to the teleseimic P-waves that is not yet attenuated. On Figure 4 we compare two band pass filterings: between 2-8 Hz (see Figure 4B) as in Figure 3 and between 5 and 15 Hz (see Figure 4A) on the traces recorded at station ATLI. The result clearly shows that the high frequency filtering suppresses the high frequency P-wave but keeps the high frequency tremors associated to the S, Love and Rayleigh waves which confirms the teleseimic origin of the high frequency energy associated to P-wave (see Figure 4). Figure 4 also exhibits a small local earthquake (see Figure 3) recorded in the same time window which has been located at the southeast boundary of the Guerrero state by the SSN network.

Higher energy tremor bursts are associated with the large-amplitude surface waves. The Love waves trigger a 80s duration tremor burst. The Rayleigh waves trigger a more complex tremor, made of successive bursts embedded in a continuous sustained activity, for a total duration of about 10 minutes. A careful look at the envelope of these bursts (Figure 3A, purple trace) shows a temporal decrease of their energies and durations. The variation of duration of the burst with time suggests a possible relation with the dispersion of the incoming long period signal. The envelope of the high frequency tremor is high-pass filtered at 10s in order to emphasize the burst activity within the

126 tremor (Figure 3A, red trace). The S-transform spectrogram [*Stockwell et al.*, 1996] of this trace is
127 then computed and compared with the S-transform spectrograms obtained from the raw data
128 recorded at UNM station (white contours) on the transverse (Figure 3C) and vertical (Figure 3D)
129 components after taking into account the distance between the two sensors. The envelope of the
130 burst triggered by the Love wave has an impulsive character and a duration of 50 seconds while the
131 successive bursts triggered by the Rayleigh waves present modulations with an increasing frequency
132 of their envelope with time. This particular frequency pattern has to be compared with the
133 dispersion of the surface waves emitted by the Maule earthquake. As expected for a mostly oceanic
134 path, the Love wave recorded at UNM station is characterized by a non-dispersive signal (the
135 Gutenberg phase) similar to the envelope of the corresponding tremor burst. On the contrary, the
136 time frequency pattern observed in the envelope of tremors (color plot) associated with the Rayleigh
137 waves (Figure 3D) mimics the strong dispersion of these waves. This shows a clear modulation of the
138 tremor activity by the dispersed Rayleigh waves. The presence of both Love and Rayleigh dispersion
139 features in tremor envelopes indicates a strong modulation of the tremors sources by the passing
140 surface waves that enhance and inhibit tremor bursts accordingly to the stress changes carried out
141 by the teleseismic waves.

142

143 3.2 Tremor activity during the first 12h after the Maule earthquake

144 In the previous subsection, we showed that the direct surface waves emitted by the Maule
145 earthquake trigger and control the tremor activity of the Guerrero gap. It has been shown that the
146 multiple surface waves of the Chile earthquake triggered microearthquakes [*Jay et al.*, 2012; *Peng et*
147 *al.*, 2011]. Here we investigate the possibility of a triggering of tremor activity by the multiple surface
148 waves (R2, R3, L2, L3) that are recorded at UNM during the 12 hours following the Maule
149 earthquake. Figure 5A presents the spectrogram analysis of the G-GAP mini-array ATLI data (Figure
150 5B presents the corresponding envelopes) for the 12 hours after the Maule earthquake and reveals
151 several periods of tremor activity around 9h, 10h, 14h and 16h (UTC). They present higher energy
152 tremors during a longer duration. The strong energy pattern visible at 7h50 is not a tremor but the
153 arrival of the T phase, which is an acoustic wave propagating in the "SOFAR channel" with a 5 Hz
154 dominant frequency [*Okal*, 2008]. For comparison, Figures 5C and 5D show the signals recorded at
155 transverse and vertical components of the UNM station (low-passed at 0.01 Hz).
156 This temporal comparison reveals that first two periods of activity (9h UT and 10h UT) correspond to
157 the arrivals of multiple surface waves that travel along the great circle. The tremor activity at 9h is
158 associated with the R2 waves (see Figure S3 in supplementary materials for a detailed comparison).

159 Similarly, the strong 10h tremor activity is correlated to the L3 and R3 arrivals (see Figure S4 for a
160 detailed comparison). At the same time, very strong and long-duration tremor episodes at 14 and 16
161 hours, are not associated with particular multiple surface waves. This indicates that after triggering
162 by the first direct surface waves (R1, L1) and a few multiples surface waves (R2, L3, R3), the tremor
163 activity continues as a process independent of the triggering waves.

164

165 3.3 Locating sources of non-volcanic tremors

166 Seismic tremors are difficult to locate because of the lack of clear impulsive wave arrivals. Several
167 different techniques are used to overcome this difficulty [*Ghosh et al.*, 2009a; *Husker et al.*, 2010;
168 *Kostoglodov et al.*, 2010; *Obara*, 2002; *Ryberg et al.*, 2010; *Shelly and Hardebeck*, 2010]. With these
169 techniques, it was possible to prove tremor migration, along strike of the subduction zones [*Obara*,
170 2002; *Obara and Sekine*, 2009; *Shelly et al.*, 2007], but also downdip or updip in the Cascadia
171 subduction zone [*Ghosh et al.*, 2009a; *Ghosh et al.*, 2010; *Ide*, 2010]. In this study, we have an
172 opportunity to investigate the possibility of tremor migration during their triggering by teleseismic
173 waves. We analyze the epicenters of the two types of tremors (the direct instantaneous triggering by
174 the incoming waves and ambient activity several hours after the passage of surface waves). Note that
175 the subduction interface is almost horizontal in the central part of the region of study. The locations
176 are obtained by two different methods.

177 The first one is a slightly modified version of the envelope cross correlation method (ECC) [*Obara*,
178 2002]. It uses the data recorded on both SSN and G-GAP networks. After the initial computation of
179 the envelope functions, we high pass filter these envelopes to extract the burst variations (see Figure
180 3A red trace). We then compute the correlations of these high pass filtered envelops. As the low
181 frequency content of the envelopes has been removed, the cross correlation functions present the
182 time delay with a single and short duration peak, which allows a better picking of the maximum of
183 the correlation. We then locate the tremors using the relative time delays and a 1D S wave velocity
184 model proposed by *Campillo et al.*, [1996].

185 The second method uses the array data and a linear beamforming approach similar to [*Ghosh et al.*,
186 2009a; *Ryberg et al.*, 2010; *Ueno et al.*, 2010]. The processing technique assumes local plane waves
187 over the array and applies a delay-and-sum approach for a range of horizontal slownesses. This
188 method provides the directions of the coherent waveform from the tremor signal selected on a given
189 time window (here 30 seconds with 50% overlap). The beamforming algorithm is usually performed
190 in the frequency domain. We first compute the cross-spectral density matrix K of the data:

$$K_{ij}(\omega) = d_i(\omega) \cdot d_j^*(\omega) \tag{1}$$

where $d_i(\omega)$ is the data recorded at sensor c_i and d_i^* is the transpose and conjugate of d_i. Then we create synthetics data $e_i(\theta,v,\omega)$ (called the replica) for a synthetic source located at a given azimuth θ from the array for an assumed velocity model *v*.

$$e_i(\theta,v,\omega) = \exp\left(i2\pi\omega \frac{\left(X_i \sin(\theta) + Y_i \cos(\theta)\right)}{v} \right) \tag{2}$$

where θ is the azimuth between the synthetic source and the array and (X_i,Y_i) is the position of the sensor c_i. Finally, we calculate the correlation between the data and the replica. If the data and the replica are perfectly coherent, the semblance value P is 1. The results for each frequency are summed to obtain the semblance between the data and the replica for a specific frequency range.

$$P(\theta,v) = \sum_{\omega} \left| e^* \cdot K \cdot e \right| \tag{3}$$

By testing all the possible azimuth and apparent velocities, the ambiguity function $P(\theta,v)$ indicates the probability of presence of the dominant noise source in terms of azimuth θ and apparent velocity. In order to increase the contrast of the ambiguity surface, the beamforming may also be performed coherently from the correlation functions of the seismic noise data [*Cros et al.*, 2011]. The ambiguity surfaces for all mini-arrays are then combined with a geometrical average to build the probability of presence of the source $PT(x_j,y_j)$ at each position (x_j,y_j).

$$PT(x_j,y_j) = \sqrt[N]{\prod_{i=1}^{N} P_i(\theta_i,V)} \tag{4}$$

with N the number of arrays, θ_i the azimuth between the point (x_j,y_j) and the array c_i and V a range of apparent velocities (here we choose all the velocities above the S-wave velocity). Finally, we apply a threshold on each probability map (0.6) to detect and locate the tremors. An example of the method is presented in Figure S5 in the supplementary materials. The location errors are of a few kilometers when the source is inside the cluster of arrays. When the sources are located outside the cluster at moderate distances (between 0 and 50 km), the locations errors are about 10 km. For sources at about 100 km from the network, the resolution decreases with a mean error of about 25 km.

Figure 6A presents the location map of the tremor for a 10 minutes time window after the S waves arrivals obtained with the two methods (ECC for the Love and the first Rayleigh wave associated

burst of tremor (inverse triangle) and beamforming for successive 30s time windows (color dots)). Despite a slight difference in latitude (beamforming locations appears closer to the coast than the ECC locations), both methods indicate that the tremors triggered by the first surface waves occur near the border between Guerrero and Oaxaca states, close to the TLIG station (blue dots and black inverse triangle in Figure 6A). This station shows the highest recorded amplitude of the tremors, which is consistent with a closer location to the source (see Figure S6). This instantaneous triggered tremor activity occurs in a region where no tremors have been reported previously. This zone corresponds to the patch that slips during the second subevent of the 2009/2010 SSE in Guerrero (see part 4 or *Walpersdorf et al.*, [2011] for a detailed description of the SSE). The sources then migrate in the northwest direction in the previously observed tremor zone [*Kostoglodov et al.*, 2010; *Payero et al.*, 2008]. This migration is characterized by a fast propagation velocity (about 125 km in 5 minutes which is about 400 m/s). Figure 6B presents, by comparison, the location of tremors within the first day without the first 20 minutes presented on Figure 6A. The location is stable for tremors associated with multiple surface waves (9h UT and 10h UT) and uncorrelated tremors (14h UT and 16h UT). The sources are located in central Guerrero, which corresponds to the previously observed tremor zone [*Kostoglodov et al.*, 2010; *Payero et al.*, 2008].

4. Triggering of a Slow Slip Event by the Mw 8.8 Chile earthquake

As seen in section 3.2, the correlation and modulation of tremor activity observed for the direct surface waves is progressively lost with time. At the first glance, it seems to exist a preserved correlation between R2, L3, R3 and fresh upsurges of tremor activity, but modulation is not visible anymore. After the passage of R3, even this apparent correlation is lost and the strong tremor activity observed at 14h UT and 16h UT on the same day is not associated with multiple surface waves (Figure 5).

We hypothesize that this qualitative change in the tremor activity may be related to some triggered deformation process at work, like slow slip, in the central Guerrero region. Indeed, *Walpersdorf et al.*, [2011] describes the occurrence of a complex SSE in 2009-2010 in the form of a double event. We re-analyze the displacements observed at the surface using various GPS stations located in Guerrero and Oaxaca states. Figure 7 presents the GPS time series for 5 GPS stations located in central and eastern Guerrero for a sample rate of 1 position per day. The time series are calculated between 2007 (after the 2006 SSE in Guerrero [*Radiguet et al.*, 2011; *Vergnolle et al.*, 2010]) and the beginning of May, 2011 assuming a fixed North America plate. On IGUA, MEZC, and ACYA stations we can clearly see the onset of an SSE in July 2009 developing until the end of 2009 when the interseismic

loading is recovered. The time of the Maule earthquake (vertical black line on Figure 7) marks the start of the second slip episode. By contrast the two other stations (CPDP and DOAP) present only the second part of slip-event that starts at the time of the Maule earthquake. These results shed a new light on the description on the 2009-2010 SSE in Mexico by *Walpersdorf et al.*, [2011]. When the Maule earthquake occurs, the 2009 first sub-event already occurred, that increased the shear stress in the southern part of the Guerrero segment. This zone is then shaken by the seismic waves and evolves towards slip instability. Our results suggest that the Maule earthquake has triggered the second large event of the 2009-2010 SSE. Despite a very precise analysis [*Vergnolle et al.*, 2010; *Walpersdorf et al.*, 2011], the noisy residuals of the GPS time series make it difficult to determine with precision (day and hour) the onset of the slow slip. We conducted a kinematic analysis (with a sampling rate of 10s), as well as a static analysis using shorter sessions (6h, 8h and 12h). Unfortunately, the results obtained do not allow determining the onset of the slip more precisely than the results for 24h session (and sampling rate of 30s) presented here. A better time resolution can be achieved with seismological records, if, accordingly with our hypothesis, we use the tremor activities as a proxy to the evolution of slow slip at depth. Figure 8 presents the energy of the seismic records at the array ATLI from February 23 to March 3, filtered between 2 and 8 Hz. This particular frequency band is the one where the activity of tremors is the most marked. We compute the average energy on 1-minute time windows. The influence of local earthquakes that may contribute in this frequency band is discarded by applying a median filter to the computed energies (with medians calculated on 30 minutes time windows). Doing so, we keep only the signals with long durations associated with tremors [*Husker et al.*, 2010]. Before the Maule earthquake (Figure 8, red vertical line), almost no tremor activity can be recorded. On the February 27, 2010, starting at the time of the P waves arrival, the tremor activity shows a 50-fold increase. The four first peaks in the tremor activity are described in Figure 5A. Interestingly, the days following the earthquake present a sustained activity of tremors, with 2 to 5 peaks of activity per day. The maximum of activity is reached on March 2, 2010, three days after the Maule earthquake with a day-long strong tremor activity. Such a sustained activity suggests a continuing deformation at depth, most likely related to the second sub-event of the SSE.

5. SSE and Tremors

In this section we discuss the possible link between the slow slip history observed with GPS and the associated tremor activity. Figure 9A presents the energy of the tremors recorded at the G-GAP arrays from March 2009 to January 2011, filtered between 2 and 8Hz. As we are only interested in

283 the long-term variations of the tremor activity, we average the energy on a 24h time window. This
284 explains why the variations of the energy during a day visible in Figure 8 are no more visible in Figure
285 9A. We clearly see the NVT burst triggered by the Chile earthquake at 2010.16 (labeled 0). This
286 tremor episode has a total duration of about 10 days. Interestingly, we observed five other NVT
287 episodes during the 2010 triggered SSE (labeled as 1, 2 3 4, and 5), and four other NVT episodes
288 (labeled -1 -2 -3 -4) between June and December 2009, during the first sub-event of the 2009-2010
289 SSE. Their durations range between 2 to 50 days with a mean recurrent time of about 50 days. The
290 time distribution of seismic tremors during the 2010 SSE is similar to the one associated with the
291 2006 SSE where four large distinct NVT episodes were recorded [*Kostoglodov et al.*, 2010].

292 In Figure 9B we compare the GPS time series (IGUA in blue and MEZC in red) with the tremor activity
293 (gray shaded areas, extracted from Figure 9A with a threshold of 0 dB). The 2 GPS stations exhibit
294 some variations in the displacement rate during the 2009-2010 SSE. The tremor 0 triggered by the
295 Maule Earthquake is associated to an acceleration of motion to the South, interpreted as a slip
296 acceleration at depth. We question now the generalization of this behavior for all the tremor
297 episodes. By visual inspection of Figure 9B, this seems to be the case for Tremor episodes -3, 1, 3, 4,
298 5. In order to confirm the link between slip rate evolution and tremor activity, we compute the
299 derivative of smoothed GPS time series in order to obtain the evolution of movement velocity at the
300 surface. Figures 9C-D present the results for the GPS stations IGUA and MEZC, which are the closest
301 to the seismic array ATLI where the tremors are observed. The velocity measured at the surface
302 confirms the previous visual analysis. The tremor episodes correspond to negative peaks in the
303 movement velocity measured in IGUA (Figure 9C) and MEZC (Figure 9D), which is a slip towards the
304 South. On the opposite, positive velocities (associated with a slip towards the North) correspond to
305 periods of relative quiescence concerning the tremor activity, at the exception of the tremor episode
306 of November 2009. These observations suggest that the tremors activity is controlled by the slow slip
307 evolution. Similar results have recently been obtained in friction experiments where a correlation
308 between the onset of slip acceleration and the emission of tremor-like signals has been observed
309 [*Zigone et al.*, 2011]. These authors show that tremor-like signals are emitted when the shear stress
310 and/or the dilatation are at maximum. They propose that the temporary increase of stress induced
311 by the rupture front propagation itself can trigger seismic tremors in zones where the stress state is
312 close to its maximum. However, the spatial link between slow slip and tremors is not so clear in
313 Mexico. *Kostoglodov et al.*, [2010] show that the two phenomena are spatially separated in the 2006
314 SSE with a tremors zone located further north from the trench compared to the SSE zone. For the
315 2009/2010 SSE, *Walpersdorf et al.*, [2011] also models a slip dislocation on two segments of the
316 subduction interface located between 70 to 100 km from the trench (see red and blue ellipses on

317 Figure 6A and 6B), further south compared to the main zone of tremors between Iguala and Mezcala
318 [*Kostoglodov et al.*, 2010].
319
320

321 **6. Discussion**

322 6.1 Triggered tremors and Modulation

323 The Mw 8.8 Maule earthquake in February 2010 triggered an intricate sequence of NVT activity in
324 Guerrero, Mexico. The first NVTs appear as single short duration bursts of tremors associated with
325 the oscillations of the incoming teleseismic shear body arrivals (S, ScS, SS). The coincidence of the
326 shear perturbations and the emergence of burst of tremors suggest that these phases generate
327 conveniently oriented shear stresses variations that trigger burst of tremors of preferred oriented
328 slip zones as proposed previously by *Rubinstein et al.*, [2007]. However, due to the depth
329 uncertainties, it is impossible to conclude on the locations of the tremor sources: it could be on the
330 slab interface at 40 km depth or on conveniently oriented surfaces in the continental crust as
331 suggested by the previously located tremors in Guerrero [*Payero et al.*, 2008].
332
333 After the body waves, a strong tremor activity is associated with the surface waves. These tremors
334 present higher energies and longer duration, which indicates a higher level of perturbations, carried
335 out by the incoming surface waves compared to the body waves. Clear modulation of tremor activity
336 is evident in the strong bursts of tremor during the passage of large long-period Rayleigh waves.
337 Modulations of tremors by surface waves has already been observed in several studies, associated
338 with the dilatations produce by the Rayleigh waves [*Miyazawa and Mori*, 2005; 2006] or by the shear
339 stresses produced by Love waves [*Rubinstein et al.*, 2007]. These authors show that the tremor turns
340 on when there are positive dilatations for Rayleigh waves and up-dip shear perturbations for Love
341 waves and turns off during compressions and down dip shear perturbations [*Miyazawa and Mori*,
342 2006; *Miyazawa and Brodsky*, 2008; *Rubinstein et al.*, 2007]. Such a behavior gives intermittent
343 tremor activities with burst of tremors when perturbations (dilatations or up-dip shear) are positive
344 and no signal when perturbations are negative. This behavior differs from what we observe in
345 Mexico during the passage of Rayleigh waves. In our case, the tremor activity is more continuous
346 with a background activity of tremor. The intensity is enhanced during positive dilatations associated
347 with the Rayleigh waves. This continuous aspect of the NVT is another evidence for a more global
348 destabilization produced by the triggered SSE is at work in Guerrero.
349

Our results show that the instantaneous triggering associated with surface waves is a short-term process. The dispersion features of the surface waves directly control the duration of the tremor bursts as shown by the S-transform analysis as discussed is Section 3.1. Moreover, in Guerrero the NVTs triggered and modulated by the surface waves present a fast migration. By comparison the ambient "long term" activity of tremor during the first day (see tremor activity in Figure 5) reveals longer duration bursts of tremor with a persistent location in central Guerrero (see locations in Figure 6B). This observation is in agreement with a recent study in Japan [*Obara*, 2010] where tremors triggered and modulated by the tide present short duration and fast migrations compared to the ambient tremor with longer duration and stable locations. However, *Obara et al.*, [2010] observed a depth discrepancy between short-term and long-term tremor locations along the plate interface. The short-term tremors are located downdip of the area of the long-term tremor, along the subduction zone, which can be explained as the demarcation between the free-sliding and the transition zone. In our case, the NVT locations are at the same distance from the trench for both types of tremor. One possible explanation comes from the geometry of the subduction interface in central Guerrero, which remains horizontal from 80 km to 200 km from the coast and has a stronger dip in eastern Guerrero (Figure 1). The zone of tremor is less affected by frictional strength weakening with increasing depth due to the thermal condition like in other subduction zones. A transition from coupled to uncoupled interface is still present in Guerrero, but this transition could be more extended due to lower temperature gradient along the plate interface [*Manea et al.*, 2004]. The consequences of such a geometry is that the possible variations in physical properties could be as strong along the strike as perpendicular to the trench, which may explain the migration from southeast to northwest of the "short-term" triggered tremors associated with surface waves.

Our analysis reveals that two types of tremors are triggered in Guerrero by the Maule earthquake. The first type is associated to the body and surface waves and presents a strong modulation. These tremors are not located in the previously detected tremor zone [*Kostoglodov et al.*, 2010; *Payero et al.*, 2008]. Interestingly, this new zone of tremors corresponds to the patch that slips during the second subevent of the 2009/2010 SSE which is triggered by the Maule earthquake (Figure 6A). This spatial correspondence and the continuous aspects of the Rayleigh wave triggered tremors indicate a deformation of that part of the subduction zone due to the triggering of the SSE. The second type of tremors is located in the previously observed tremor zone in Guerrero [*Kostoglodov et al.*, 2010; *Payero et al.*, 2008] and is triggered by the variations in the slip evolution of the SSE. Figure 9 shows that the tremors are stronger at the peaks of movement velocity in the south direction. We may then suppose that, at the first order, tremor activity is concomitant with period of large strain rate, which

383 is similar to the behavior observed for the seismic velocity changes in the crust during the 2006 SSE
384 by *Rivet et al.*, [2011].

385

386 6.2 Triggering of SSE and Tremors by Large Distant Earthquakes

387 Large distant earthquakes are known to trigger earthquakes either by static or dynamic triggering [*Di*
388 *Carli et al.*, 2008; *Freed*, 2005; *Gomberg and Johnson*, 2005; *Gomberg et al.*, 2001; *Gomberg et al.*,
389 2004; *Hill et al.*, 1993; *King et al.*, 1994; *Marsan and Lengline*, 2008; *Stein et al.*, 1994; *Voisin et al.*,
390 2004]. More recently, it has been shown that large distant earthquakes can also trigger tremor
391 activity down dip the subduction zones [*Miyazawa and Mori*, 2005; 2006; *Rubinstein et al.*, 2007;
392 *Rubinstein et al.*, 2009] and along continental faults [*Ghosh et al.*, 2009b; *Gomberg et al.*, 2008; *Peng*
393 *et al.*, 2008; *Shelly et al.*, 2011]. It was proposed also that teleseismic events could trigger ETS
394 [*Rubinstein et al.*, 2009], and here we have shown that the Maule earthquake triggered a large slow
395 slip event associated with a enhanced tremor activity.

396 In the period 2009-2011, other large teleseismic earthquakes have been recorded in Mexico. Here
397 we select the 26 earthquakes with a magnitude above 7 that have been recorded at the station ATLI
398 between November 2009 (date of the installation) and March 2011. None of these earthquakes
399 triggered tremors nor SSE in Guerrero. Figure 10A show the spectral content of these earthquakes on
400 the vertical component. The color lines present the spectra for the events that produced the four
401 largest Peak Ground Velocity (PGV) at ATLI (see Table 1 for a list of the earthquakes and the PGV).
402 The red line is for the Maule earthquake. The three other events (Haiti, Mexicali and Tohoku-Oki) did
403 not trigger any tremors or SSE (see Figure 9 and Figure 10A). In the following we will focus on these 3
404 events compared to the Maule earthquake to discuss the possible constraints on the potential of a
405 large earthquake to trigger tremors and/or SSE.

406 Numerous studies have focused on the triggering of aftershocks and/or stable sliding on continental
407 faults [*Gomberg and Johnson*, 2005; *Gomberg et al.*, 2001; *Voisin et al.*, 2004]. It emerges that the
408 potential for triggering depends on the balance between the loading parameters (namely frequency
409 and amplitude) and the intrinsic mechanics of the fault (friction law, state of stress).

410 Figures 10B and 10C present the spectral ratios of the Maule earthquake over the 3 other
411 earthquakes (details given in Table 2) for the vertical and transverse components measured at UNM.
412 They reveal that the energy of the long periods surface waves are 2 to 4 orders of magnitude greater
413 for the Maule earthquake between 10s and 1000s on the two components with respect to Haïti and
414 Mexicali earthquakes. When compared to Tohoku-Oki rupture, these ratios drops in the range 1-100;

Indeed the Maule and Tohoki-Oki ruptures have similar magnitudes, and the ratio tends to be 1 at longer periods. The discrepancy at higher frequencies is related to the shorter epicentral distance of Maule earthquake.

From this spectral analysis, we can infer that the potential of an earthquake to trigger a SSE or tremors depends on its spectral content at long periods. This is particularly underscored by the Haïti and the Mexicali earthquakes that are depleted in energy above 10s. Indeed, even if the Mexicali earthquake produces high dynamic stresses in Guerrero (12.5 kPa see table 1) the frequency content is to high to trigger tremors or SSE. To verify this observation we calculate the PGV and the corresponding dynamic stresses on 30-100 seconds band pass filtered traces for all earthquakes (see table 1). Only two events emerge: the Maule (11.37 kPa) and Tohoku-Oki (4.26 kPa) earthquakes. This result is consistent with what is known for the potential of triggering of aftershocks and/or stable sliding: amplitudes at long periods are more likely to trigger activity [*Gomberg and Johnson*, 2005; *Guilhem et al.*, 2010; *Hill et al.*, 1993; *Voisin*, 2001; 2002].

The case of Tohoku-Oki earthquake seems to contradict this result, as it has quite the same spectral content as the Maule earthquake and therefore could trigger also SSE and tremor activity. The absence of triggered activity can be related to the fact that after June 2010, most of the subduction interface prone to SSEs in Guerrero had already slipped. It is an unloaded interface that was subject to the passing of the high amplitude seismic waves. As expected from simple frictional models, the initial conditions at the plate interface seem to be a controlling factor for the triggering by long period waves. However note that the precision of GPS measurements prevents the detection of SSEs with magnitude smaller than 6.5. Our argument is therefore based also on the absence of observable tremor burst.

These three earthquakes help to constrain the conditions for SSE/ tremor triggering: it is controlled by both the amplitude of the incoming waves and by the state of stress on the interface. Large perturbation with significant long period energy to trigger SSE suggests that a critical length exists like for dynamic triggering of earthquakes [*Andrews*, 1976; *Dascalu et al.*, 2000; *Uenishi and Rice*, 2003; *Voisin*, 2001; 2002]. The fault has to be stressed in a region large enough for the instability to grow. Note that the energy of the Chile signal is larger than for the Haïti event for period larger than 10s, that is for wavelength longer that 40km at least. This suggests that a large part of the subduction zone in Guerrero has to be solicited by large amplitudes long periods waves to trigger SSE.

7. Conclusions

We observe that both SSE and tremors were triggered in Guerrero by the 2010 Mw 8.8 Maule earthquake. First, we detected tremors triggered in Guerrero by the passing S, Love and Rayleigh waves of the Maule earthquake. The greatest amount of tremor energy and duration accompanies the long-period Rayleigh waves, with smaller tremor bursts during the S and Love waves. For the Rayleigh wave triggered tremor, we observed the dispersion of Rayleigh waves in the envelopes of the tremor energy, which indicates a strong modulation of the tremor source by the passing surface waves. Secondly, the analysis of the GPS time series suggests that the second sub-event of the 2009-2010 slow slip event in Guerrero is actually triggered by the Maule earthquake. The displacement in the south direction started coincidently with the earthquake within the GPS resolution. Tremors started immediately with the arrival of the waves and lasted for a period much longer that the duration of the seismic waves, indicating a continuing process we identify as the SSE second sub-event.

The link between NVTs and SSE is illustrated by the comparison between GPS time series and tremor activity during 2010. While it is known that tremors are not permanently active during the SSEs, neither located in the zone of largest slip [*Kostoglodov et al.*, 2010], tremors bursts are observed when GPS time series exhibit a component of motion towards the South, indicating some slip at depth.

We investigated the conditions of triggering by examining the behavior of the subduction during different large earthquakes. Not surprisingly, we found that the triggering of significant NVTs is controlled by both the amplitude of the incoming waves and by the state of stress on the interface. The observation of a large SSE triggered by a distant large earthquake is an important indication of a possible global mechanism of interaction between major active structures. A large SSE actually affects significantly the elastic stress on the subduction interface, including the seismogenic zone. In the months after the Maule earthquake, and its triggering effect, the state of stress increased in the coupled zone of the Guerrero subduction segment. Indeed this effect is delayed by the time necessary for the development of a transient creep event, that is several months and this stress increase has no direct impact so far, except possibly advancing the clock for the next earthquake.

It was recently discussed in various meetings that very large earthquakes during the last century exhibit some form of temporal clustering. Indeed the statistical significance of the observation on such a short time window can be questioned [*Michael*, 2011]. In any case, the deterministic process responsible for such a clustering is unclear. A simple conceptual model of global clustering can be derived from the observation in Guerrero after the Maule earthquake. Our specific observation suggests that large slow slip events are triggered by mega earthquakes on the global scale, some of

480 them being ignored with the resolution of our instrumentation, particularly in the past. They affect
481 the stress level of the seismogenic parts of subduction interfaces, producing a clustering of events
482 worldwide. The observations we present here indicate that the amplitude of the low frequency
483 waves is a control parameter of the triggering process, with a positive trigger with the Mw8.8 Maule
484 earthquake. This suggests that only mega earthquakes can trigger SSE at the global scale, and have
485 the potential to produce temporal clustering of large earthquakes on the scale of a few years.

486

487 **Acknowledgments:**

488 This study was supported by the Agence Nationale de la Recherche (France) under the contract
489 RA0000CO69 (G-GAP) and by project grants from CONACYT 84544 and PAPIIT IN110611, IN103808.
490 UNM station is operated by GEOSCOPE (geoscope.ipgp.fr). We are grateful to all the participants to
491 the G-GAP field works. We thank Paul Johnson, Yehuda Ben-Zion, Fabrice Cotton, Michel
492 Bouchon, Cécile Lasserre, Erwan Pathier, Guillaume Bacques, Victor Cruz-Atienza and François
493 Renard for discussions. We also thank the Associate Editor and two anonymous reviewers for their
494 constructive reviews.

495

496

497 **References:**

498 Andrews, D. J. (1976), RUPTURE PROPAGATION WITH FINITE STRESS IN ANTIPLANE STRAIN, *Journal*
499 *of Geophysical Research*, *81*(20), 3575-3582.

500 Brown, K. M., M. D. Tryon, H. R. DeShon, L. M. Dorman, and S. Y. Schwartz (2005), Correlated
501 transient fluid pulsing and seismic tremor in the Costa Rica subduction zone, *Earth and Planetary*
502 *Science Letters*, *238*(1-2), 189-203.

503 Campillo, M., S. Singh, N. Shapiro, J. Pacheco, and R. Herrmann (1996), Crustal structure south of the
504 Mexican volcanic belt, based on group velocity dispersion, *Geofisica Internacional*, *35*, 361.

505 Chao, K., Z. G. Peng, C. Q. Wu, C. C. Tang, and C. H. Lin (2012), Remote triggering of non-volcanic
506 tremor around Taiwan, *Geophysical Journal International*, *188*(1), 301-324.

507 Cotte, N., A. Walpersdorf, V. Kostoglodov, M. Vergnolle, J.-A. Santiago, I. Manighetti, and M. Campillo
508 (2009), Anticipating the next large silent earthquake in Mexico, *Eos Trans. AGU*, *90*(21), 181-182.

509 Cros, E., P. Roux, J. Vandemeulebrouck, and S. Kedar (2011), Locating hydrothermal acoustic sources
510 at Old Faithful Geyser using Matched Field Processing, *Geophysical Journal International*, *187*(1), 385-
511 393.

512 Dascalu, C., I. R. Ionescu, and M. Campillo (2000), Fault finiteness and initiation of dynamic shear
513 instability, *Earth and Planetary Science Letters*, *177*(3-4), 163-176.

514 DeMets, C., R. G. Gordon, and D. F. Argus (2010), Geologically current plate motions, *Geophysical*
515 *Journal International*, *181*(1), 1-80.

516 Di Carli, S., C. Voisin, F. Cotton, and F. Semmane (2008), The 2000 western Tottori (Japan)
517 earthquake: Triggering of the largest aftershock and constraints on the slip-weakening distance,
518 *Journal of Geophysical Research-Solid Earth*, *113*(B5).

519 Dragert, H., K. L. Wang, and T. S. James (2001), A silent slip event on the deeper Cascadia subduction
520 interface, *Science*, *292*(5521), 1525-1528.

521 Freed, A. M. (2005), Earthquake triggering by static, dynamic, and postseismic stress transfer, *Annual*
522 *Review of Earth and Planetary Sciences*, *33*, 335-367.

523 Ghosh, A., J. E. Vidale, J. R. Sweet, K. C. Creager, and A. G. Wech (2009a), Tremor patches in Cascadia
524 revealed by seismic array analysis, *Geophysical Research Letters*, *36*.

525 Ghosh, A., J. E. Vidale, Z. G. Peng, K. C. Creager, and H. Houston (2009b), Complex nonvolcanic
526 tremor near Parkfield, California, triggered by the great 2004 Sumatra earthquake, *Journal of*
527 *Geophysical Research-Solid Earth*, *114*.

528 Ghosh, A., J. E. Vidale, J. R. Sweet, K. C. Creager, A. G. Wech, and H. Houston (2010), Tremor bands
529 sweep Cascadia, *Geophysical Research Letters*, *37*.

530 Gomberg, J., and P. Johnson (2005), Seismology - Dynamic triggering of earthquakes, *Nature*,
531 *437*(7060), 830-830.

532 Gomberg, J., P. A. Reasenberg, P. Bodin, and R. A. Harris (2001), Earthquake triggering by seismic
533 waves following the Landers and Hector Mine earthquakes, *Nature*, *411*(6836), 462-466.

534 Gomberg, J., P. Bodin, K. Larson, and H. Dragert (2004), Earthquake nucleation by transient
535 deformations caused by the M=7.9 Denali, Alaska, earthquake, *Nature*, *427*(6975), 621-624.

536 Gomberg, J., J. L. Rubinstein, Z. G. Peng, K. C. Creager, J. E. Vidale, and P. Bodin (2008), Widespread
537 triggering of nonvolcanic tremor in California, *Science*, *319*(5860), 173-173.

538 Guilhem, A., Z. G. Peng, and R. M. Nadeau (2010), High-frequency identification of non-volcanic
539 tremor triggered by regional earthquakes, *Geophysical Research Letters*, *37*.

540 Hill, D. P., et al. (1993), SEISMICITY REMOTELY TRIGGERED BY THE MAGNITUDE 7.3 LANDERS,
541 CALIFORNIA, EARTHQUAKE, *Science*, *260*(5114), 1617-1623.

542 Hirose, H., K. Hirahara, F. Kimata, N. Fujii, and S. Miyazaki (1999), A slow thrust slip event following
543 the two 1996 Hyuganada earthquakes beneath the Bungo Channel, southwest Japan, *Geophysical*
544 *Research Letters*, *26*(21), 3237-3240.

545 Husker, A., S. Peyrat, N. Shapiro, and V. Kostoglodov (2010), Automatic non-volcanic tremor
546 detection in the Mexican subduction zone, *Geofisica Internacional*, *49*(1), 17-25.

Husker, A. L., V. Kostoglodov, V. M. Cruz-Atienza, D. Legrand, N. M. Shapiro, J. S. Payero, M. Campillo, and E. Huesca-Perez (2012), Temporal variations of non-volcanic tremor (NVT) locations in the Mexican subduction zone: Finding the NVT sweet spot, *Geochemistry Geophysics Geosystems*, *13*.

Ide, S. (2010), Striations, duration, migration and tidal response in deep tremor, *Nature*, *466*(7304), 356-U105.

Itaba, S., and R. Ando (2011), A slow slip event triggered by teleseismic surface waves, *Geophysical Research Letters*, *38*.

Jaeger, J. C., and N. G. W. Cook (1979), *Fundamentals of Rock Mechanics*, 3rd edn ed., Chapman and Hall, New York, NY.

Jay, J. A., M. E. Pritchard, M. E. West, D. Christensen, M. Haney, E. Minaya, M. Sunagua, S. R. McNutt, and M. Zabala (2012), Shallow seismicity, triggered seismicity, and ambient noise tomography at the long-dormant Uturuncu volcano, *Bolivia, Bull. Volcanology*.

Kim, Y., R. W. Clayton, and J. M. Jackson (2010), Geometry and seismic properties of the subducting Cocos plate in central Mexico, *Journal of Geophysical Research-Solid Earth*, *115*, 22.

King, G. C. P., R. S. Stein, and J. Lin (1994), STATIC STRESS CHANGES AND THE TRIGGERING OF EARTHQUAKES, *Bulletin of the Seismological Society of America*, *84*(3), 935-953.

Kostoglodov, V., W. Bandy, J. Dominguez, and M. Mena (1996), Gravity and seismicity over the Guerrero seismic gap, Mexico, *Geophysical Research Letters*, *23*(23), 3385-3388.

Kostoglodov, V., S. K. Singh, J. A. Santiago, S. I. Franco, K. M. Larson, A. R. Lowry, and R. Bilham (2003), A large silent earthquake in the Guerrero seismic gap, Mexico, *Geophysical Research Letters*, *30*(15), 4.

Kostoglodov, V., A. Husker, N. M. Shapiro, J. S. Payero, M. Campillo, N. Cotte, and R. Clayton (2010), The 2006 slow slip event and nonvolcanic tremor in the Mexican subduction zone, *Geophysical Research Letters*, *37*, 5.

Linde, A. T., M. T. Gladwin, M. J. S. Johnston, R. L. Gwyther, and R. G. Bilham (1996), A slow earthquake sequence on the San Andreas fault, *Nature*, *383*(6595), 65-68.

Manea, V. C., M. Manea, V. Kostoglodov, C. A. Currie, and G. Sewell (2004), Thermal structure, coupling and metamorphism in the Mexican subduction zone beneath Guerrero, *Geophysical Journal International*, *158*(2), 775-784.

Marsan, D., and O. Lengline (2008), Extending earthquakes' reach through cascading, *Science*, *319*(5866), 1076-1079.

Michael, A. J. (2011), Random variability explains apparent global clustering of large earthquakes, *Geophysical Research Letters*, *38*.

Miyazawa, M., and J. Mori (2005), Detection of triggered deep low-frequency events from the 2003 Tokachi-oki earthquake, *Geophysical Research Letters*, *32*(10), 4.

Miyazawa, M., and J. Mori (2006), Evidence suggesting fluid flow beneath Japan due to periodic seismic triggering from the 2004 Sumatra-Andaman earthquake, *Geophysical Research Letters*, *33*(5), 4.

585 Miyazawa, M., and E. E. Brodsky (2008), Deep low-frequency tremor that correlates with passing
586 surface waves, *Journal of Geophysical Research-Solid Earth*, *113*(B1), 17.

587 Obara, K. (2002), Nonvolcanic deep tremor associated with subduction in southwest Japan, *Science*,
588 *296*(5573), 1679-1681.

589 Obara, K. (2010), Depth-dependent activity of non-volcanic tremor and other slow earthquake in the
590 Nankai subduction zone, in *AGU Fall Meeting Abstracts*, edited by AGU, p. 05.

591 Obara, K., and S. Sekine (2009), Characteristic activity and migration of episodic tremor and slow-slip
592 events in central Japan, *Earth Planets and Space*, *61*(7), 853-862.

593 Obara, K., S. Tanaka, T. Maeda, and T. Matsuzawa (2010), Depth-dependent activity of non-volcanic
594 tremor in southwest Japan, *Geophysical Research Letters*, *37*.

595 Ohta, Y., J. T. Freymueller, S. Hreinsdottir, and H. Suito (2006), A large slow slip event and the depth
596 of the seismogenic zone in the south central Alaska subduction zone, *Earth and Planetary Science*
597 *Letters*, *247*(1-2), 108-116.

598 Okal, E. A. (2008), The generation of T waves by earthquakes, in *Advances in Geophysics, Vol 49*,
599 edited, pp. 1-65, Elsevier Academic Press Inc, San Diego.

600 Outerbridge, K. C., T. H. Dixon, S. Y. Schwartz, J. I. Walter, M. Protti, V. Gonzalez, J. Biggs, M.
601 Thorwart, and W. Rabbel (2010), A tremor and slip event on the Cocos-Caribbean subduction zone as
602 measured by a global positioning system (GPS) and seismic network on the Nicoya Peninsula, Costa
603 Rica, *Journal of Geophysical Research-Solid Earth*, *115*.

604 Pardo, M., and G. Suarez (1995), SHAPE OF THE SUBDUCTED RIVERA AND COCOS PLATES IN
605 SOUTHERN MEXICO - SEISMIC ANTI TECTONIC IMPLICATIONS, *Journal of Geophysical Research-Solid*
606 *Earth*, *100*(B7), 12357-12373.

607 Payero, J. S., V. Kostoglodov, N. Shapiro, T. Mikumo, A. Iglesias, X. Perez-Campos, and R. W. Clayton
608 (2008), Nonvolcanic tremor observed in the Mexican subduction zone, *Geophysical Research Letters*,
609 *35*(7).

610 Peng, Z. G., and K. V. Chao (2008), Non-volcanic tremor beneath the Central Range in Taiwan
611 triggered by the 2001 M-w 7.8 Kunlun earthquake, *Geophysical Journal International*, *175*(2), 825-
612 829.

613 Peng, Z. G., C. Q. Wu, and C. Aiken (2011), Delayed triggering of microearthquakes by multiple
614 surface waves circling the Earth, *Geophysical Research Letters*, *38*.

615 Peng, Z. G., J. E. Vidale, A. G. Wech, R. M. Nadeau, and K. C. Creager (2009), Remote triggering of
616 tremor along the San Andreas Fault in central California, *Journal of Geophysical Research-Solid Earth*,
617 *114*.

618 Peng, Z. G., J. E. Vidale, K. C. Creager, J. L. Rubinstein, J. Gomberg, and P. Bodin (2008), Strong tremor
619 near Parkfield, CA, excited by the 2002 Denali Fault earthquake, *Geophysical Research Letters*,
620 *35*(23).

621 Perez-Campos, X., Y. Kim, A. Husker, P. M. Davis, R. W. Clayton, A. Iglesias, J. F. Pacheco, S. K. Singh,
622 V. C. Manea, and M. Gurnis (2008), Horizontal subduction and truncation of the Cocos Plate beneath
623 central Mexico, *Geophysical Research Letters*, *35*(18).

Peterson, C. L., and D. H. Christensen (2009), Possible relationship between nonvolcanic tremor and the 1998-2001 slow slip event, south central Alaska, *Journal of Geophysical Research-Solid Earth*, *114*.

Radiguet, M., F. Cotton, M. Vergnolle, M. Campillo, B. Valette, V. Kostoglodov, and N. Cotte (2011), Spatial and temporal evolution of a long term slow slip event: the 2006 Guerrero Slow Slip Event, *Geophysical Journal International*, *184*(2), 816-828.

Rivet, D., M. Campillo, N. M. Shapiro, V. Cruz-Atienza, M. Radiguet, N. Cotte, and V. Kostoglodov (2011), Seismic evidence of nonlinear crustal deformation during a large slow slip event in Mexico, *Geophysical Research Letters*, *38*.

Rogers, G., and H. Dragert (2003), Episodic tremor and slip on the Cascadia subduction zone: The chatter of silent slip, *Science*, *300*(5627), 1942-1943.

Rubinstein, J. L., J. E. Vidale, J. Gomberg, P. Bodin, K. C. Creager, and S. D. Malone (2007), Non-volcanic tremor driven by large transient shear stresses, *Nature*, *448*(7153), 579-582.

Rubinstein, J. L., J. Gomberg, J. E. Vidale, A. G. Wech, H. Kao, K. C. Creager, and G. Rogers (2009), Seismic wave triggering of nonvolcanic tremor, episodic tremor and slip, and earthquakes on Vancouver Island, *Journal of Geophysical Research-Solid Earth*, *114*.

Ryberg, T., C. Haberland, G. S. Fuis, W. L. Ellsworth, and D. R. Shelly (2010), Locating non-volcanic tremor along the San Andreas Fault using a multiple array source imaging technique, *Geophysical Journal International*, *183*(3), 1485-1500.

Schwartz, S. Y., and J. M. Rokosky (2007), Slow slip events and seismic tremor at circum-pacific subduction zones, *Reviews of Geophysics*, *45*(3).

Shelly, D. R., and J. L. Hardebeck (2010), Precise tremor source locations and amplitude variations along the lower-crustal central San Andreas Fault, *Geophysical Research Letters*, *37*.

Shelly, D. R., G. C. Beroza, and S. Ide (2007), Complex evolution of transient slip derived from precise tremor locations in western Shikoku, Japan, *Geochemistry Geophysics Geosystems*, *8*.

Shelly, D. R., Z. Peng, D. P. Hill, and C. Aiken (2011), Triggered creep as a possible mechanism for delayed dynamic triggering of tremor and earthquakes, *Nature Geoscience*, *4*(6), 384-388.

Stein, R. S., G. C. P. King, and J. Lin (1994), STRESS TRIGGERING OF THE 1994 M=6.7 NORTHRIDGE, CALIFORNIA, EARTHQUAKE BY ITS PREDECESSORS, *Science*, *265*(5177), 1432-1435.

Stockwell, R. G., L. Mansinha, and R. P. Lowe (1996), Localization of the complex spectrum: The S transform, *Ieee Transactions on Signal Processing*, *44*(4), 998-1001.

Uenishi, K., and J. R. Rice (2003), Universal nucleation length for slip-weakening rupture instability under nonuniform fault loading, *Journal of Geophysical Research-Solid Earth*, *108*(B1).

Ueno, T., T. Maeda, K. Obara, Y. Asano, and T. Takeda (2010), Migration of low-frequency tremors revealed from multiple-array analyses in western Shikoku, Japan, *Journal of Geophysical Research-Solid Earth*, *115*, 12.

Vergnolle, M., A. Walpersdorf, V. Kostoglodov, P. Tregoning, J. A. Santiago, N. Cotte, and S. I. Franco (2010), Slow slip events in Mexico revised from the processing of 11 year GPS observations, *Journal of Geophysical Research-Solid Earth*, *115*.

Voisin, C. (2001), Dynamic triggering of earthquakes: the linear slip-dependent friction case, *Geophysical Research Letters*, *28*(17), 3357-3360.

Voisin, C. (2002), Dynamic triggering of earthquakes: The nonlinear slip-dependent friction case, *Journal of Geophysical Research-Solid Earth*, *107*(B12).

Voisin, C., F. Cotton, and S. Di Carli (2004), A unified model for dynamic and static stress triggering of aftershocks, antishocks, remote seismicity, creep events, and multisegmented rupture, *Journal of Geophysical Research-Solid Earth*, *109*(B6).

Walpersdorf, A., N. Cotte, V. Kostoglodov, M. Vergnolle, M. Radiguet, J. A. Santiago, and M. Campillo (2011), Two successive slow slip events evidenced in 2009-2010 by a dense GPS network in Guerrero, Mexico, *Geophysical Research Letters*, *38*.

Zigone, D., C. Voisin, E. Larose, F. Renard, and M. Campillo (2011), Slip acceleration generates seismic tremor like signals in friction experiments *Geophys. Res. Lett.*, *38*, L01315.

LIST OF FIGURE AND TABLE CAPTIONS

Figure 1: Seismotectonic map of Guerrero, Mexico (after [*Kostoglodov et al.*, 2003]). Inverse yellow triangles with black contours indicate the STS2 3 components stations from the Servicio Sismológico Nacional (SSN) of Mexico. The names of these stations are indicated in black. The green dots with red contours indicate the G-GAP mini-arrays (1 CMG40 3 components sensor and 6 vertical short period sensors). The G-GAP array's names are indicated in red. The purple square is the STS1 broadband UNM Geoscope station in Mexico City. The blue triangles are the GPS stations used in this study (the names are in blue). The blue arrows indicate the direction and velocity in cm/yr of the PVEL relative plate motion between the Cocos and North American Plate [*DeMets et al.*, 2010]. Little blue patches represent the major earthquakes rupture zones. Thin gray lines show the isodepth contours of the subducted oceanic slab (after [*Pardo and Suarez*, 1995]). The insert presents the great circle path between the epicenter of Maule earthquake and UNM station in Mexico City (red line). The blue square indicates the location of the main map.

Figure 2: Section of 12 north-south seismograms obtained on the broadband sensors of the SSN and G-GAP networks. The traces are filtered between 2-8 Hz to exhibit the tremors.

Figure 3: (A) Comparison between the 2-8 Hz filtered data recorded on a short period sensor at ATLI (black trace) and the broadband record of the Chilean earthquake at the UNM station in Mexico City for the transverse (green trace) and vertical (blue trace) components. The time scale is in seconds and starts at the initial time of the Maule earthquake. The envelope function of the ATLI data is in purple. The red trace is the high pass filtered envelope function that clearly shows the variations in the tremor activity. There is a clear triggering of tremor in ATLI by the S wave packet, the Love wave and the Rayleigh wave. A careful look at the envelope of this triggered tremor (Figure3A purple trace) shows a decrease of the seismic energy radiated by the NVT bursts and a temporal decrease of their duration. This observation reveals a dispersion in the envelope of the triggered tremor. (B) Spectrogram of the data recorded at ATLI. (C and D) We compare the S-transform spectrogram obtained for the high pass filtered envelope presented in (A) (color plot) with the S-transform spectrograms obtained for the raw broadband records at UNM station (white contours). (C) show the transverse component and (D) the vertical component. The comparison of the dispersion observed in the envelope of tremors (color plot) with the one associated with Rayleigh waves recorded in Mexico City (Figure 3D) shows the modulation of the tremors by the dispersed waves.

Figure 4: (A) Data recorded on the vertical component at ATLI station and filtered between 5 and 15 Hz. (B) Same as A but filtered between 2 and 8 Hz. (C) Raw data recorded at ATLI.

Figure 5: (A) Spectrogram of the data recorded on a short-period sensor in ATLI between 0 and 10 Hz. The high energy in the 2-7 Hz frequency band corresponds to tremor activity. (B) Envelope of filtered data recorded in ATLI. (C) Transverse component of the UNM Geoscope station filtered between 100 and 1000 seconds. The multiple of Love waves L2 and L3 can be identified and correspond to tremor activity. (D) Vertical component of the UNM Geoscope station filtered between 100 and 1000 seconds. The multiples Rayleigh waves R2 and R3 are correlated to strong tremor activity. Note that the time is indicated UTC and is different from what is presented on figure 2 and 3.

Figure 6: (A) NVT location map for the short-term triggering associated with the surface waves. Inversed black triangles indicate the locations obtained with the ECC method for the tremors triggered by Love and Rayleigh waves. The dots indicate the epicenters obtained with the beamforming method. The color scale gives the time in seconds after the initial time of the Maule earthquake (see Figure 3 for the corresponding time series with the same time scale). As we focus only on surface waves, the color scale starts around 1600 seconds, just before the Love wave arrival. (B) NVT location map for the long-term triggering. Black triangles indicate the stations and color dots are tremor locations. The color scale is in hours (see Figure 5 for the corresponding envelope and spectrogram). The surface projections of the two slip patches in 2009/2010 are shown schematically by the red (2009.5) and blue (2010.15) ellipses in the bottom of the maps [*Walpersdorf et al.*, 2011].

Figure 7: GPS North-South component time series between 2007 and 2011 for various stations in central and eastern Guerrero: IGUA (blue), MEZC (red), ACYA (purple), CPDP (green) and DOAP (black). Black line stands for the Chile earthquake occurrence.

Figure 8: Energy of the seismic record between 2 and 8 Hz at the ATLI BHZ channel during 9 days between February 23, 2010 and March 3, 2010. Vertical red line presents the time of the earthquake. We clearly see the increase of the tremor activity after the earthquake. This sustained activity remains during 4 days after the earthquake with a peak on March 2, 2010, 3 days after the earthquake.

Figure 9: (A) Energy of the seismological record between 2 and 8 Hz at various BHZ channel (we combined the stations ATLI, APAX and ARIG to obtain the longest possible time series). Note that the scale is in decibels to facilitate the visualization of the evolution of tremors energy. The purple vertical lines represent the time of Haiti earthquake, Chile earthquake and Mexicali earthquake that occurred the 12^{th} of January 2010, the 27^{th} of February 2010 and the 4^{th} of April 2010 respectively. The numbers associated with each tremor episode are indicated in red. (B) Comparison between the GPS measurements and the tremor activity. The color dots are the GPS time series at 2 stations in

762 Guerrero (IGUA in blue and MEZC in red located in the same zone as the seismological sensors). The
763 black curves are the GPS time series smoothed with a moving average window of 10 days. The
764 vertical purple lines indicate the time of the Haiti, Chile and Mexicali earthquakes. The shaded areas
765 in grayscale are the tremors activities extracted from (A) with the threshold of 0 dB. **(**C, D) Derivative
766 of the smoothed GPS time series recorded at IGUA (C), MEZC (D). These curves present the surface
767 velocity, which is positive for displacement toward the north and negative in the south direction.

768 **Figure 10:** (A) Velocity Power spectral density computed from record of the 26 earthquakes recorded
769 at ATLI. The color lines represent the spectra of the earthquakes that produced the largest PGV in
770 ATLI (see table 1): Chile (red), Tohoku-Oki (black), Mexicali (blue) and Haiti (green) earthquakes. (B
771 and C) Spectral ratios between the Mw 8.8 Maule earthquake and 3 other earthquakes: Mw 7.0 Haiti
772 earthquake (blue curve), Mw 9.0 Tohoku-Oki earthquake (black curve) and Mw 7.2 Baja California,
773 Mexicali earthquakes (red curve). The four events have been recorded at the same UNM station in
774 Mexico City (for B and C).

775 **Table 1:** List of earthquakes recorded in ATLI station. The dynamic stresses are calculated
776 using the equation $\sigma_d = G\,\dot{u}/v_s$ [*Jaeger and Cook*, 1979], where G is the shear modulus, $\dot{u}$ is
777 the PGV and v_s is the phase velocity. Here we choose a generic 30 GPa shear modulus and a
778 3.5 km/s Rayleigh wave velocity [*Chao et al.*, 2012; *Miyazawa and Brodsky*, 2008]. The
779 earthquakes listed in table 2 are highlighted in gray.

780

781 **Table 2:** Characteristics of highest PGV earthquakes (see table 1 for all the earhquakes).

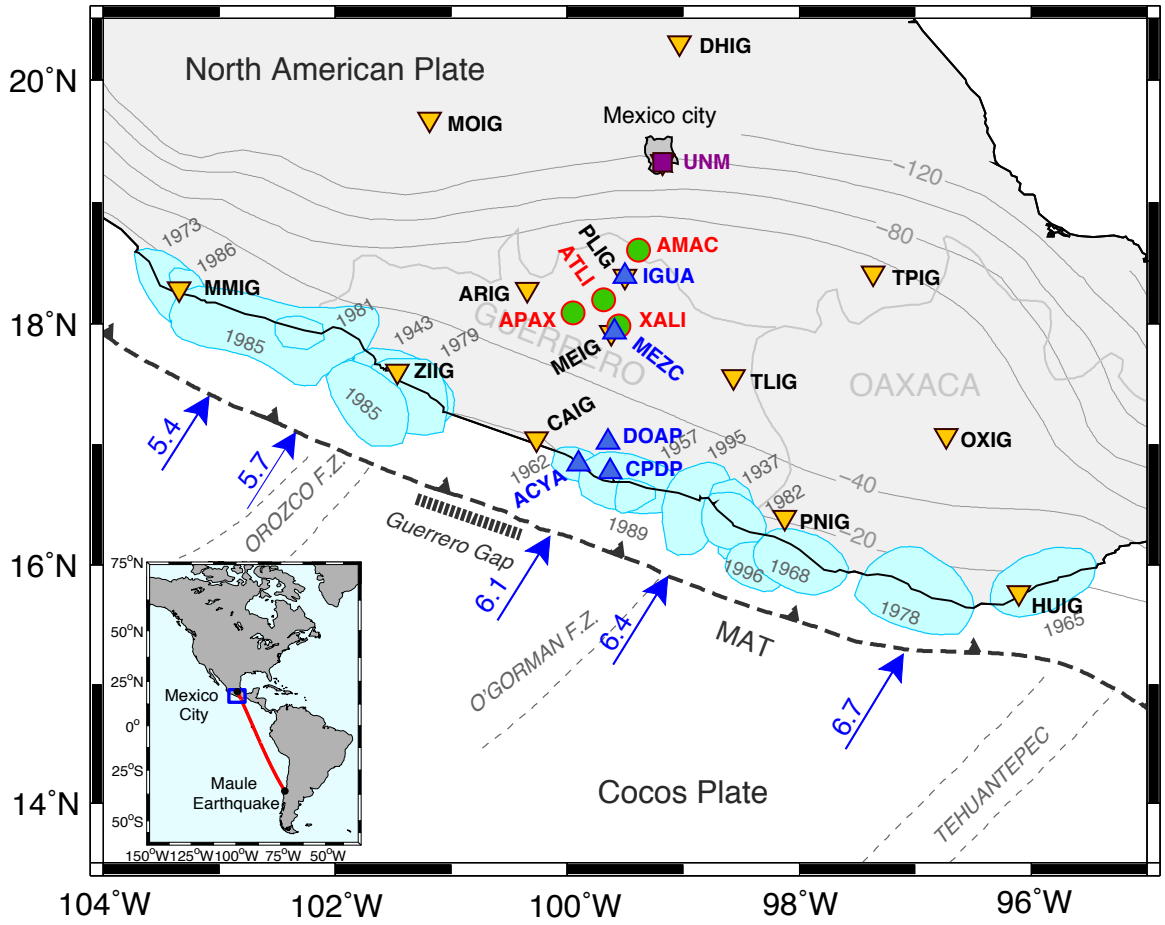

Figure 1: Seismotectonic map of Guerrero, Mexico (after [*Kostoglodov et al.*, 2003]). Inverse yellow triangles with black contours indicate the STS2 3 components stations from the Servicio Sismológico Nacional (SSN) of Mexico. The names of these stations are indicated in black. The green dots with red contours indicate the G-GAP mini-arrays (1 CMG40 3 components sensor and 6 vertical short period sensors). The G-GAP array's names are indicated in red. The purple square is the STS1 broadband UNM Geoscope station in Mexico City. The blue triangles are the GPS stations used in this study (the names are in blue). The blue arrows indicate the direction and velocity in cm/yr of the PVEL relative plate motion between the Cocos and North American Plate [*DeMets et al.*, 2010]. Little blue patches represent the major earthquakes rupture zones. Thin gray lines show the isodepth contours of the subducted oceanic slab (after [*Pardo and Suarez*, 1995]). The insert presents the great circle path between the epicenter of Maule earthquake and UNM station in Mexico City (red line). The blue square indicates the location of the main map.

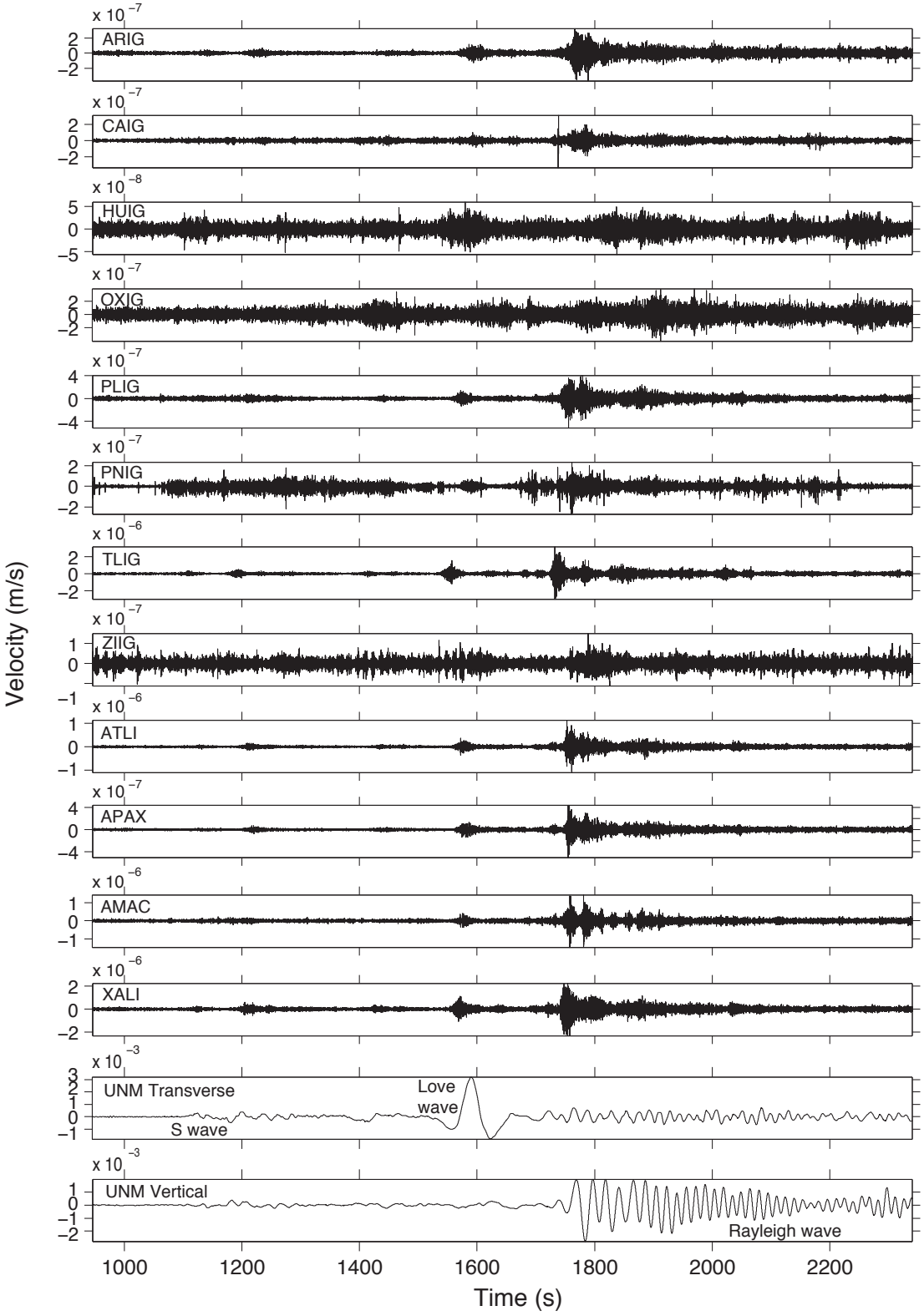

797

798 **Figure 2:** Section of 12 north-south seismograms obtained on the broadband sensors of the SSN and
799 G-GAP networks. The traces are filtered between 2-8 Hz to exhibit the tremors. At the bottom are
800 presented the raw transverse and vertical components of the UNM station in Mexico City.

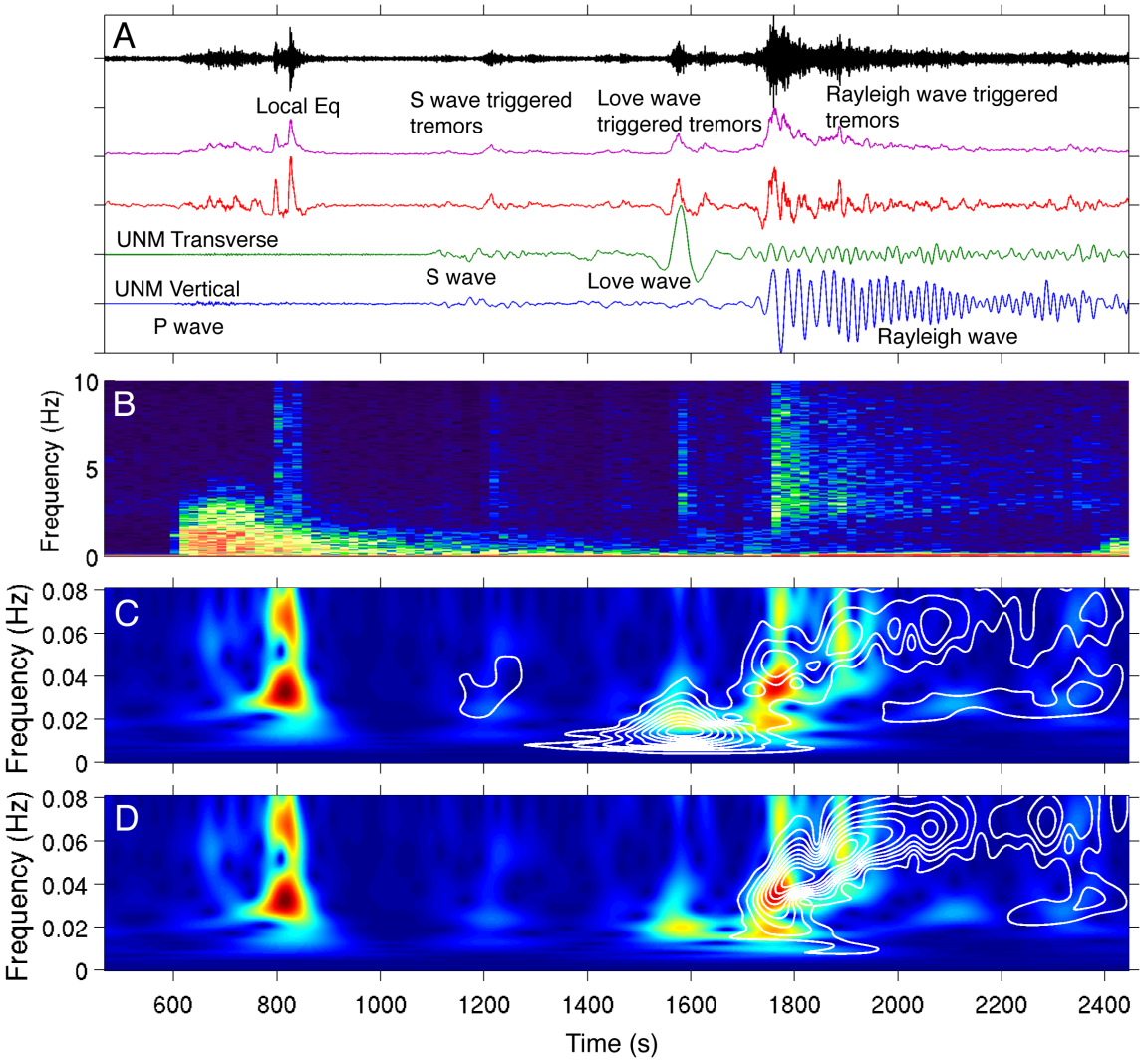

Figure 3: (A) Comparison between the 2-8 Hz filtered data recorded on a short period sensor at ATLI (black trace) and the broadband record of the Chilean earthquake at the UNM station in Mexico City for the transverse (green trace) and vertical (blue trace) components. The time scale is in seconds and starts at the initial time of the Maule earthquake. The envelope function of the ATLI data is in purple. The red trace is the high pass filtered envelope function that clearly shows the variations in the tremor activity. There is a clear triggering of tremor in ATLI by the S wave packet, the Love wave and the Rayleigh wave. A careful look at the envelope of this triggered tremor (Figure3A purple trace) shows a decrease of the seismic energy radiated by the NVT bursts and a temporal decrease of their duration. This observation reveals a dispersion in the envelope of the triggered tremor. (B) Spectrogram of the data recorded at ATLI. (C and D) We compare the S-transform spectrogram obtained for the high pass filtered envelope presented in (A) (color plot) with the S-transform spectrograms obtained for the raw broadband records at UNM station (white contours). (C) show the transverse component and (D) the vertical component. The comparison of the dispersion observed in

815 the envelope of tremors (color plot) with the one associated with Rayleigh waves recorded in Mexico
816 City (Figure 3D) shows the modulation of the tremors by the dispersed waves.
817
818
819
820
821
822
823
824
825
826
827
828
829
830
831
832
833
834
835

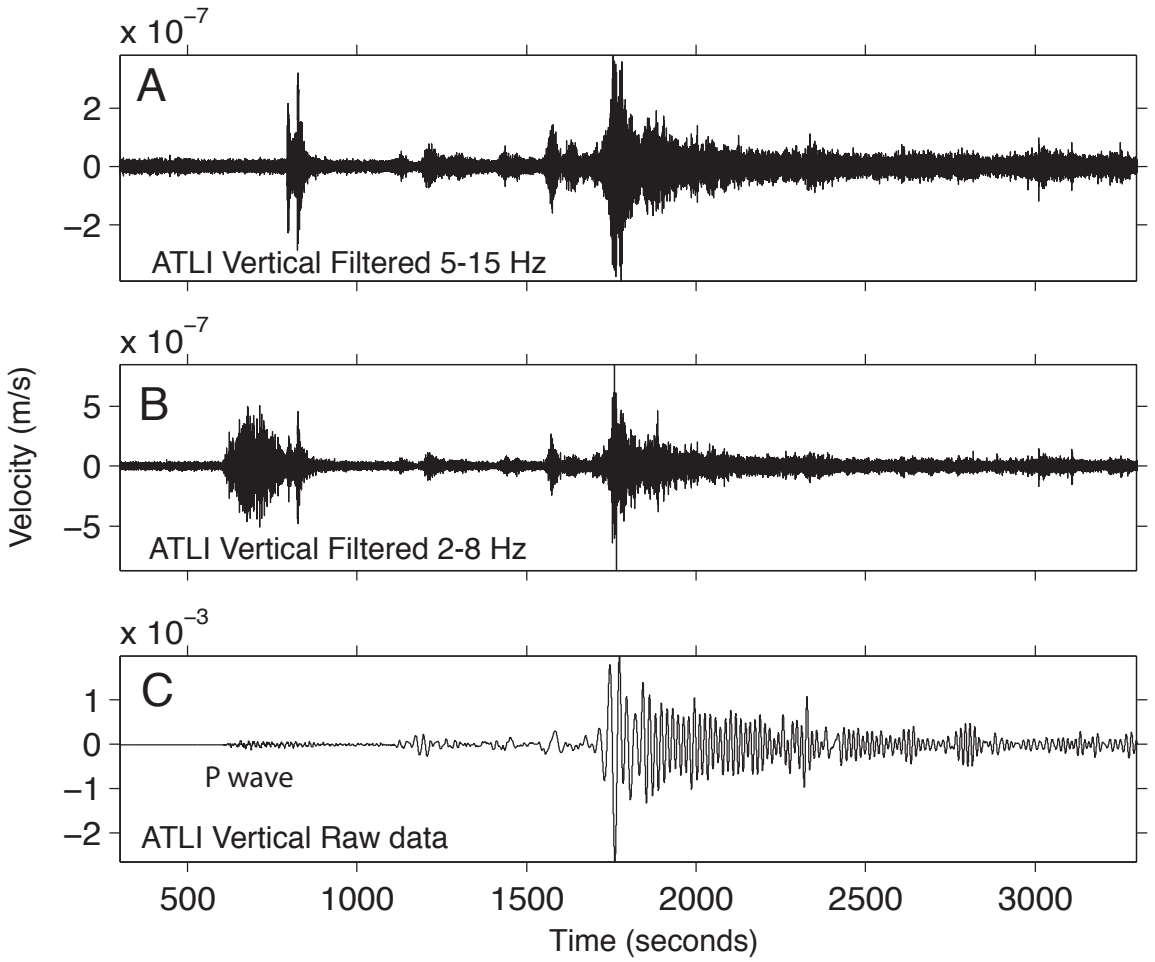

836

837 **Figure 4:** (A) Data recorded on the vertical component at ATLI station and filtered between 5 and 15

838 Hz. (B) Same as A but filtered between 2 and 8 Hz. (C) Raw data recorded at ATLI.

839

840

841

842

843

844

845

846

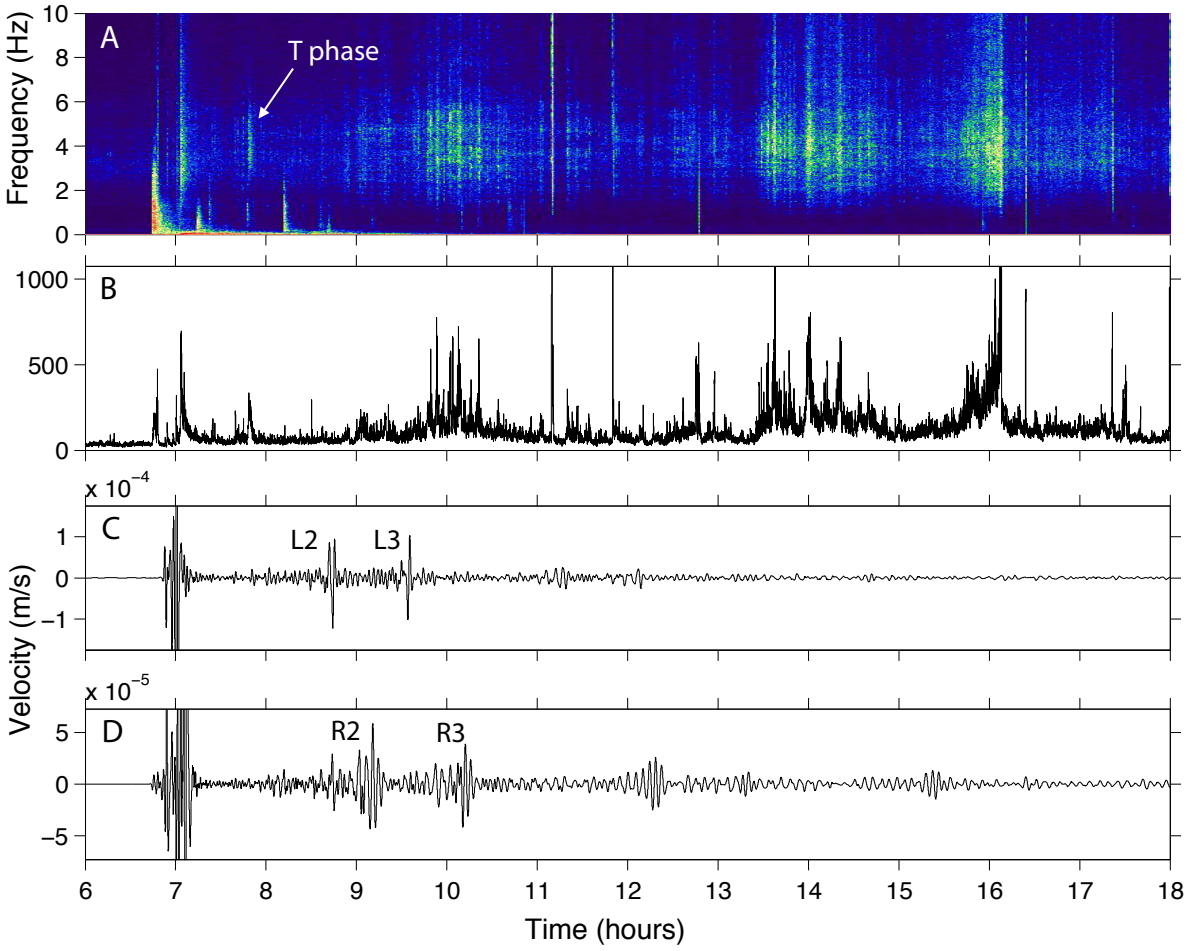

847

848 **Figure 5:** (A) Spectrogram of the data recorded on a short-period sensor in ATLI between 0 and 10
849 Hz. The high energy in the 2-7 Hz frequency band corresponds to tremor activity. (B) Envelope of
850 filtered data recorded in ATLI. (C) Transverse component of the UNM Geoscope station filtered
851 between 100 and 1000 seconds. The multiple of Love waves L2 and L3 can be identified and
852 correspond to tremor activity. (D) Vertical component of the UNM Geoscope station filtered
853 between 100 and 1000 seconds. The multiples Rayleigh waves R2 and R3 are correlated to strong
854 tremor activity. Note that the time is indicated UTC and is different from what is presented on figure
855 2 and 3.

856

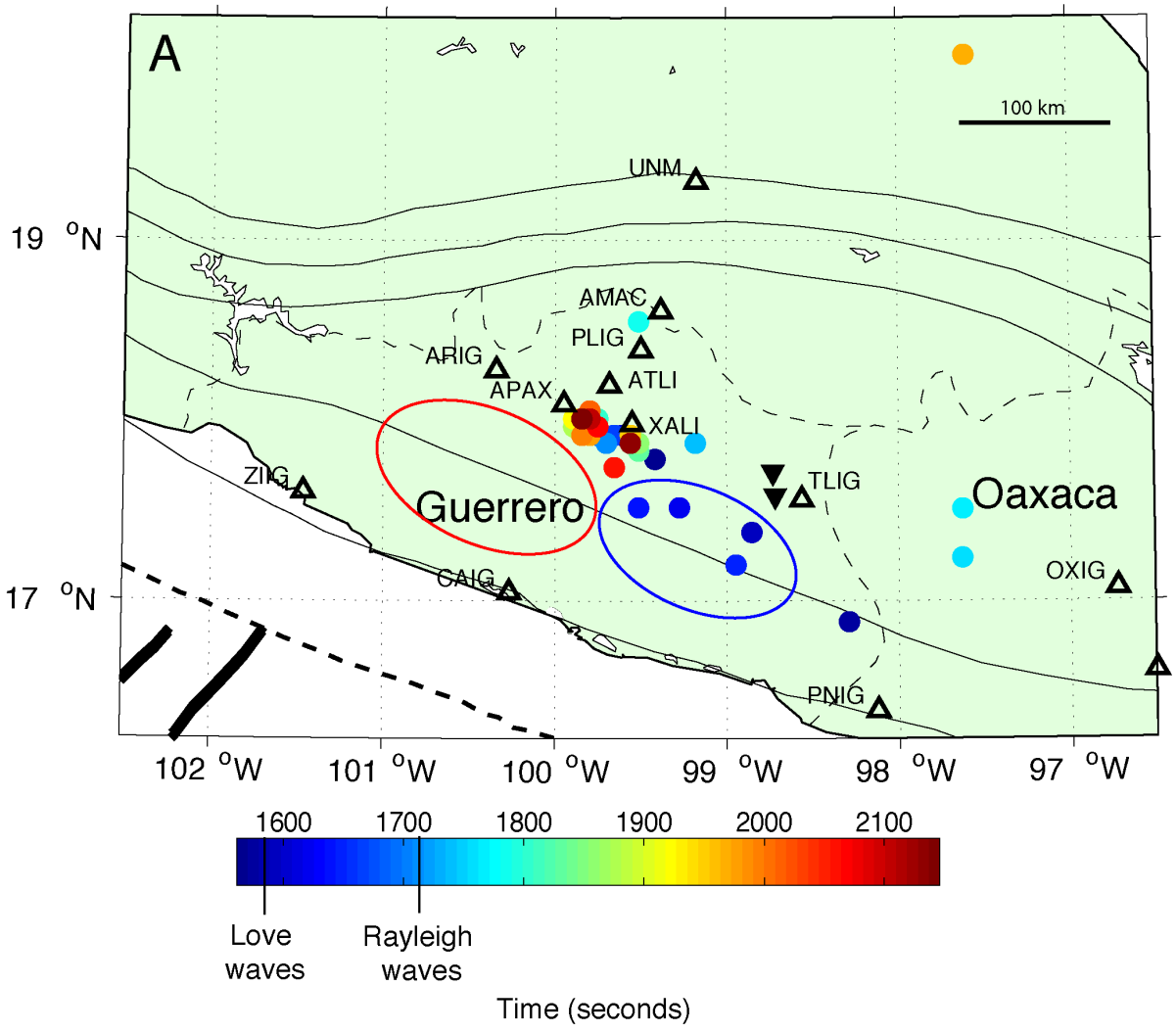

857

858 **Figure 6:** (A) NVT location map for the short-term triggering associated with the surface waves.
859 Inversed black triangles indicate the locations obtained with the ECC method for the tremors
860 triggered by Love and Rayleigh waves. The dots indicate the epicenters obtained with the
861 beamforming method. The color scale gives the time in seconds after the initial time of the Maule
862 earthquake (see Figure 3 for the corresponding time series with the same time scale). As we focus
863 only on surface waves, the color scale starts around 1600 seconds, just before the Love wave arrival.

864

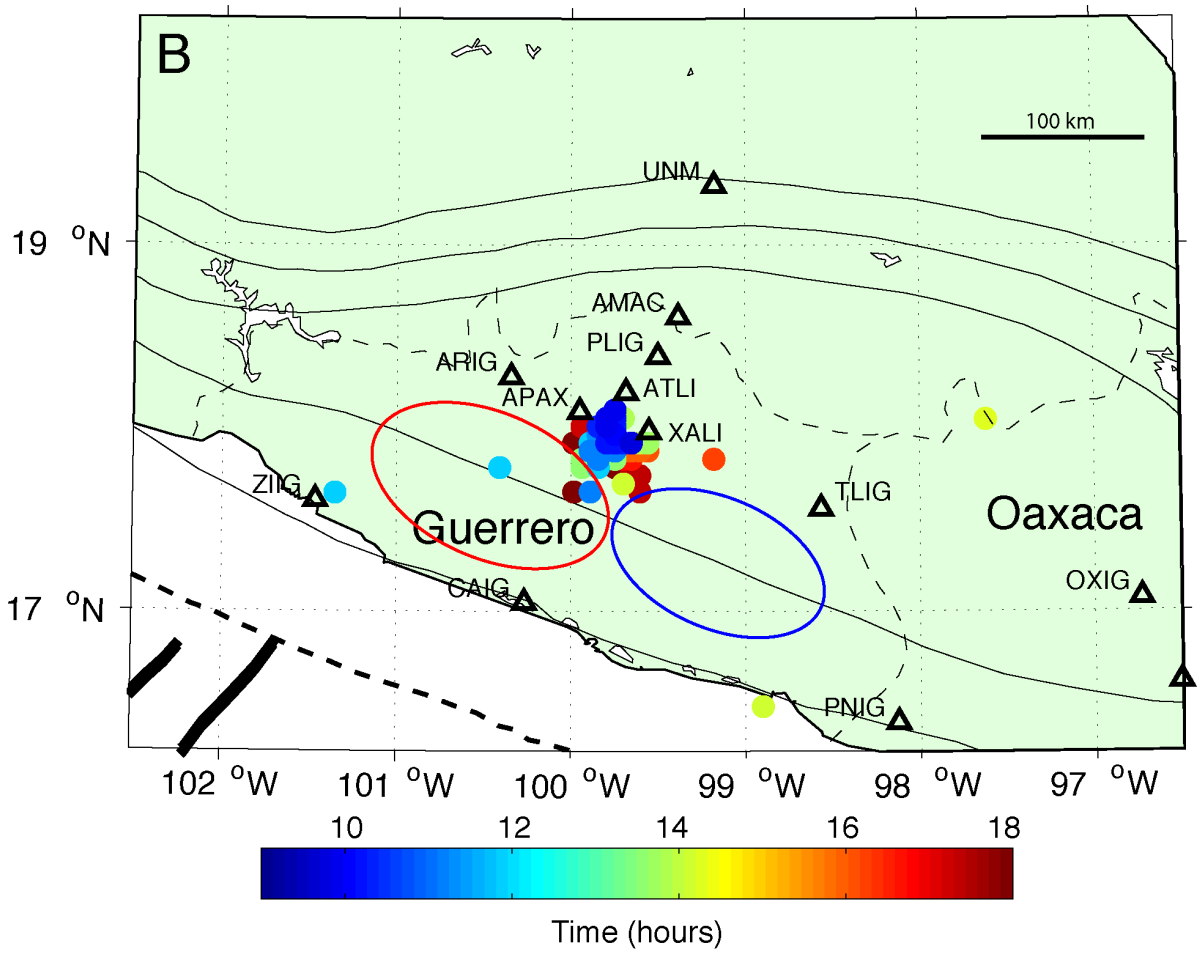

865

866 **Figure 6:** (B) NVT location map for the long-term triggering. Black triangles indicate the stations and
867 color dots are tremor locations. The color scale is in hours (see Figure 5 for the corresponding
868 envelope and spectrogram). The surface projections of the two slip patches in 2009/2010 are shown
869 schematically by the red (2009.5) and blue (2010.15) ellipses in the bottom of the maps [*Walpersdorf*
870 *et al.*, 2011].

871

872

873

874

875

876

877

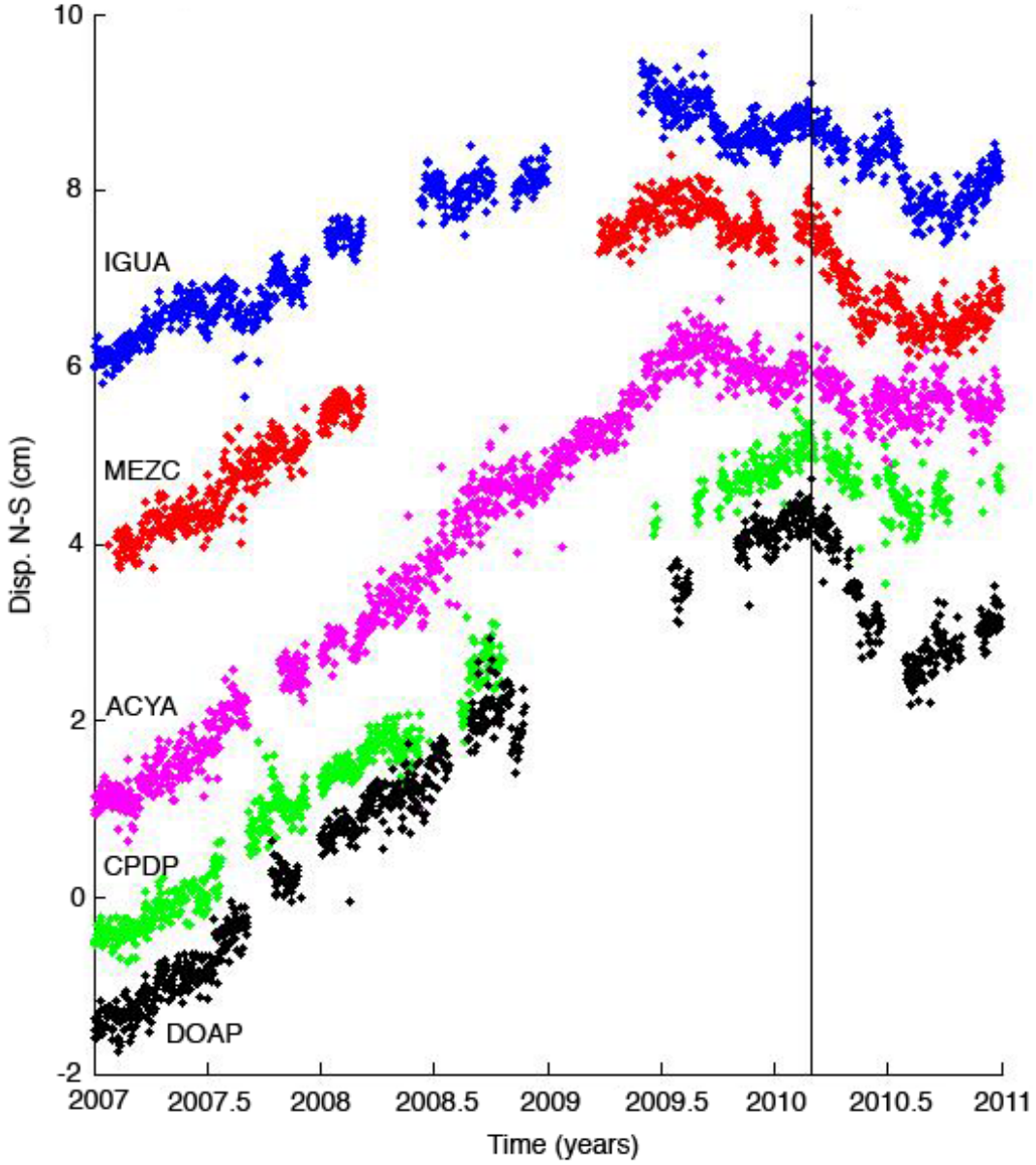

878
879 **Figure 7:** GPS North-South component time series between 2007 and 2011 for various stations in
880 central and eastern Guerrero: IGUA (blue), MEZC (red), ACYA (purple), CPDP (green) and DOAP
881 (black). Black line stands for the Chile earthquake occurrence.

882

883

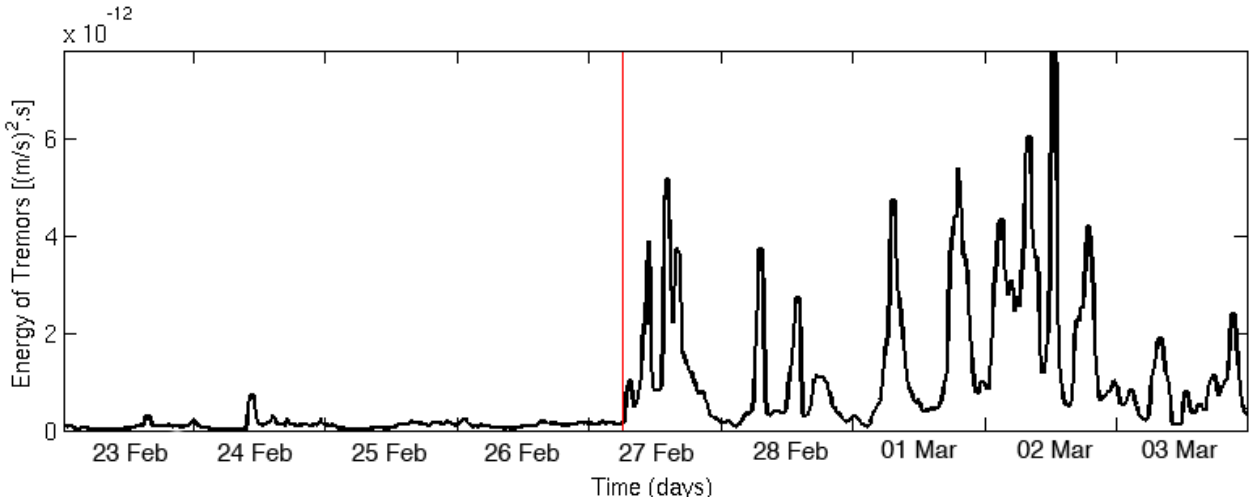

Figure 8: Energy of the seismic record between 2 and 8 Hz at the ATLI BHZ channel during 9 days between February 23, 2010 and March 3, 2010. Vertical red line presents the time of the earthquake. We clearly see the increase of the tremor activity after the earthquake. This sustained activity remains during 4 days after the earthquake with a peak on March 2, 2010, 3 days after the earthquake.

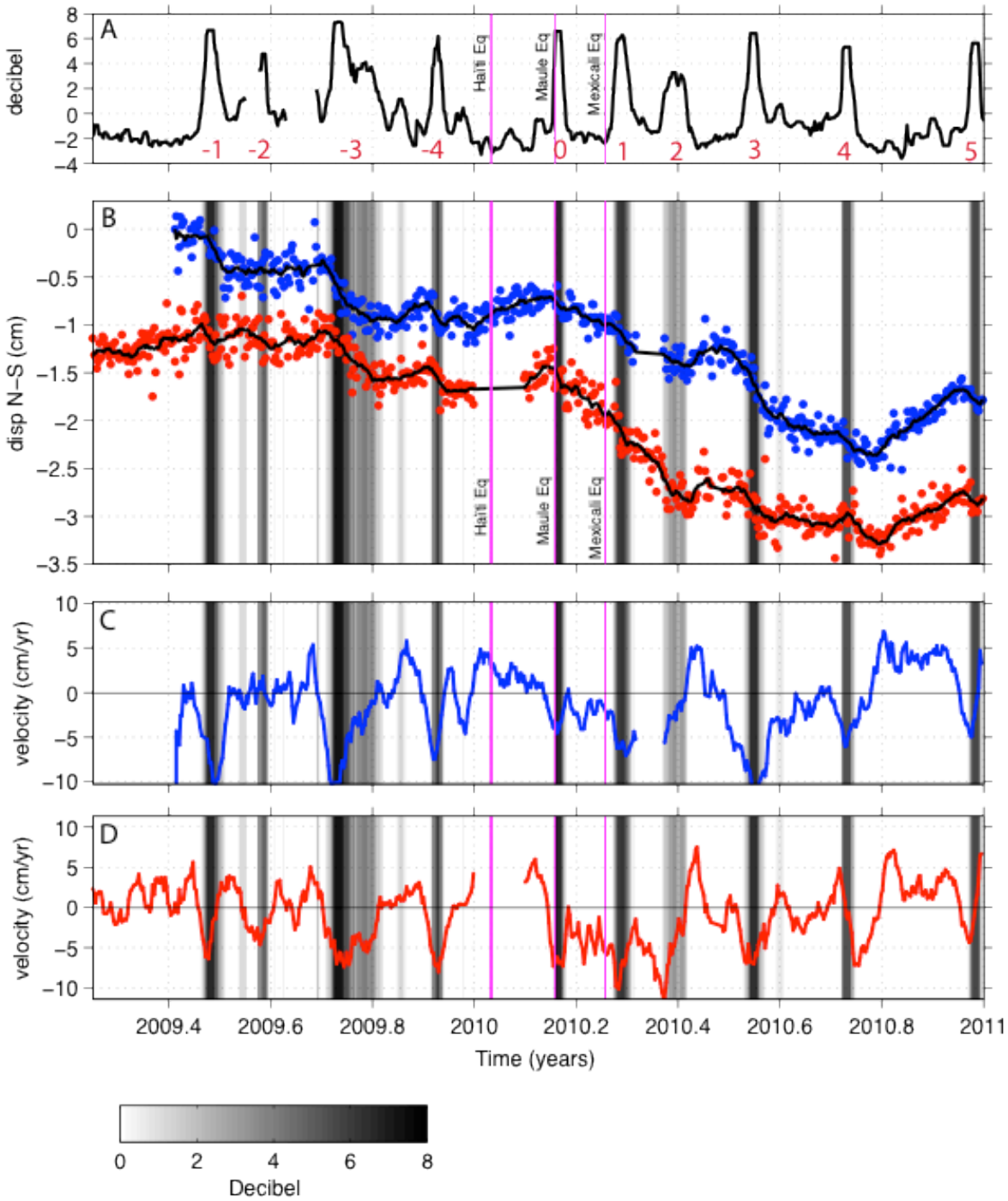

902

903 **Figure 9:** (A) Energy of the seismological record between 2 and 8 Hz at various BHZ channel (we
904 combined the stations ATLI, APAX and ARIG to obtain the longest possible time series). Note that the
905 scale is in decibels to facilitate the visualization of the evolution of tremors energy. The purple
906 vertical lines represent the time of Haiti earthquake, Chile earthquake and Mexicali earthquake that
907 occurred the 12th of January 2010, the 27th of February 2010 and the 4th of April 2010 respectively.
908 The numbers associated with each tremor episode are indicated in red. (B) Comparison between the
909 GPS measurements and the tremor activity. The color dots are the GPS time series at 2 stations in

Guerrero (IGUA in blue and MEZC in red located in the same zone as the seismological sensors). The black curves are the GPS time series smoothed with a moving average window of 10 days. The vertical purple lines indicate the time of the Haiti, Chile and Mexicali earthquakes. The shaded areas in grayscale are the tremors activities extracted from (A) with the threshold of 0 dB. **(**C, D) Derivative of the smoothed GPS time series recorded at IGUA (C), MEZC (D). These curves present the surface velocity, which is positive for displacement toward the north and negative in the south direction.

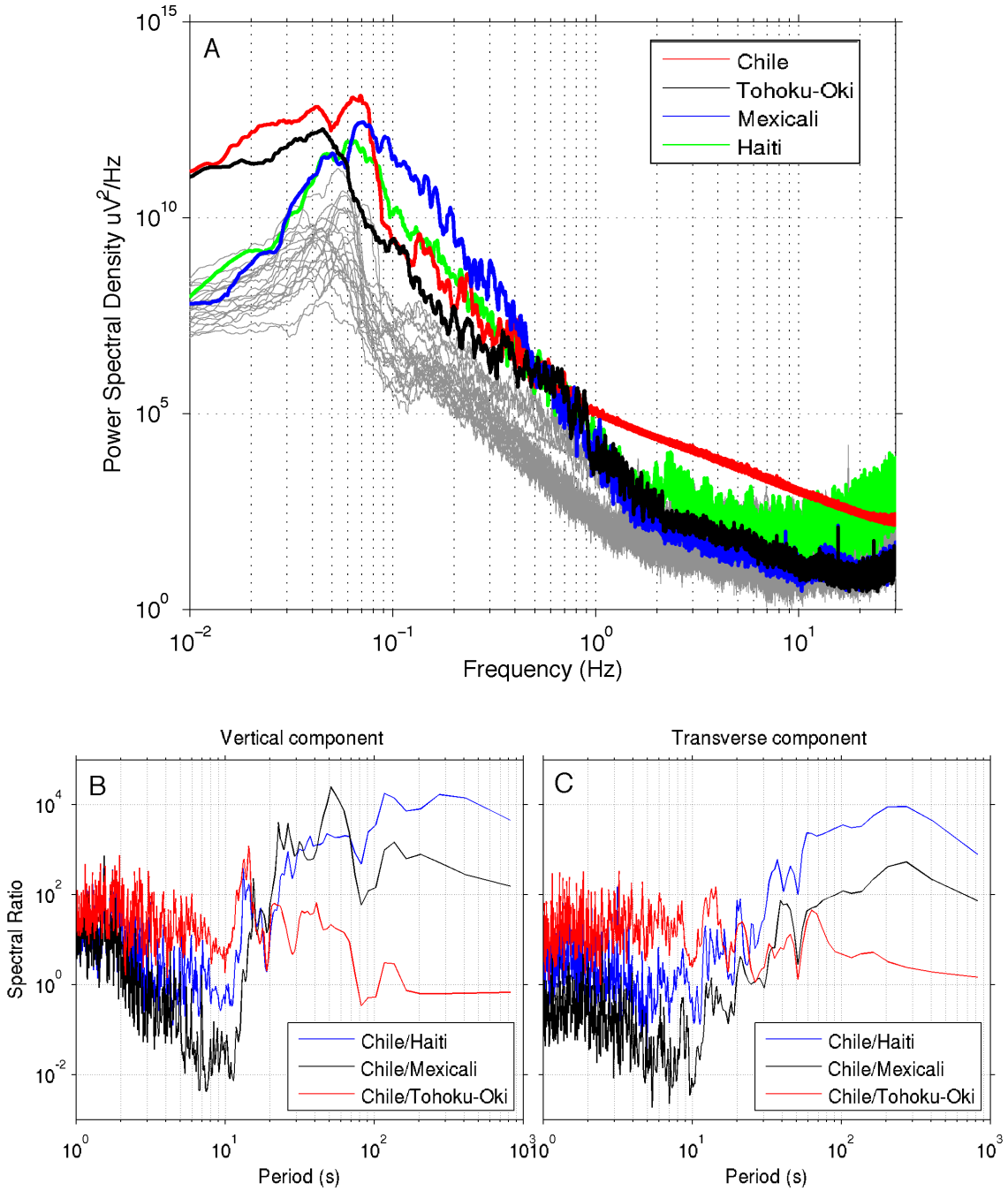

935

936 **Figure 10:** (A) Velocity Power spectral density computed from record of the 26 earthquakes recorded
937 at ATLI. The color lines represent the spectra of the earthquakes that produced the largest PGV in
938 ATLI (see table 1): Chile (red), Tohoku-Oki (black), Mexicali (blue) and Haiti (green) earthquakes. (B
939 and C) Spectral ratios between the Mw 8.8 Maule earthquake and 3 other earthquakes: Mw 7.0 Haiti
940 earthquake (blue curve), Mw 9.0 Tohoku-Oki earthquake (black curve) and Mw 7.2 Baja California,
941 Mexicali earthquakes (red curve). The four events have been recorded at the same UNM station in
942 Mexico City (for B and C).

Year	Month	Day	Hour	Lat	Long	Depth (km)	Mw	PGV (cm/s)	σ_d (kPa) (raw)	σ_d (kPa) (filtered 30-100 s)
2010	1	3	22:36:25.64	-8.78	157.35	10	7.1	0,0038	0,33	0,22
2010	1	12	21:53:10.06	18.44	-72.57	13	7.0	0,0419	3,59	0,31
2010	2	26	203126.97	25.93	128.43	25	7.0	0,0010	0,08	0,04
2010	2	27	06:34:11.53	-36.12	-72.90	22	8.8	0,2623	22,48	11,37
2010	3	11	14:55:27.51	-34.33	-71.80	18	7.0	0,0064	0,55	0,09
2010	4	4	22:40:43.10	32.30	-115.28	4	7.2	0,1458	12,50	0,72
2010	4	6	22:15:01.58	2.38	97.05	31	7.8	0,0105	0,90	0,20
2010	5	9	05:59:41.62	3.75	96.02	38	7.2	0,0033	0,28	0,08
2010	5	27	17:14:46.57	-13.70	166.64	31	7.2	0,0048	0,41	0,10
2010	6	12	19:26:50.46	7.88	91.94	35	7.5	0,0038	0,33	0,20
2010	6	16	03:16:27.55	-2.17	136.54	18	7.0	0,0013	0,11	0,02
2010	7	18	13:34:59.36	-5.93	150.59	35	7.3	0,0025	0,22	0,04
2010	7	23	22:51:12.45	6.49	123.47	585	7.6	0,0061	0,52	0,08
2010	8	4	22:01:43.62	-5.75	150.76	44	7.0	0,0011	0,09	0,02
2010	8	10	05:23:44.98	-17.54	168.07	25	7.3	0,0023	0,20	0,07
2010	8	12	11:54:15.58	-1.27	-77.31	206	7.1	0,0028	0,24	0,05
2010	9	3	16:35:47.77	-43.52	171.83	12	7.0	0,0038	0,33	0,08
2010	9	29	17:11:25.94	-4.96	133.76	26	7.0	0,0010	0,08	0,06
2010	10	25	14:42:22.46	-3.49	100.08	20	7.8	0,0022	0,19	0,06
2010	12	21	17:19:40.66	26.90	143.70	14	7.4	0,0039	0,33	0,08
2011	1	1	09:56:58.12	-26.80	-63.14	576	7.0	0,0027	0,24	0,01
2011	1	2	20:20:17.78	-38.35	-73.33	24	7.2	0,0051	0,43	0,14
2011	1	13	16:16:41.54	-20.63	168.47	9	7.0	0,0046	0,40	0,19
2011	1	18	20:23:23.48	28.78	63.95	68	7.2	0,0030	0,26	0,12
2011	3	9	02:45:20.33	38.44	142.84	32	7.3	0,0038	0,33	0,21

2011	3	11	05:46:24.12	38.20	142.37	29	9.0	0,0664	5,69	4,26

Table 1: List of earthquakes recorded in ATLI station. The dynamic stresses are calculated using the equation $\sigma_d = G\,\dot{u}/v_s$ [*Jaeger and Cook*, 1979], where G is the shear modulus, $\dot{u}$ is the PGV and v_s is the phase velocity. Here we choose a generic 30 GPa shear modulus and a 3.5 km/s Rayleigh wave velocity [*Chao et al.*, 2012; *Miyazawa and Brodsky*, 2008]. The earthquakes listed in table 2 are highlighted in gray.

	Haiti Earthquake	Maule Earthquake	Mexicali Earthquake	Tohoku-Oki Earthquake
Location	Haiti	Chile	Mexico	Japan
Date	12 Jan 2010	27 Feb 2010	04 Apr 2010	11 Mar 2011
Number of days with respect to Maule Eq	- 46	0	+ 36	+ 377
Distance from Mexico city (km)	2801	6751	2165	10963
Latitude (deg)	8.443	-35.909	32.259	38.322
Longitude (deg)	-72.571	-72.733	-115.387	142.369
Depth (km)	13	35	10	32
Mw	7.0	8.8	7.2	9.0

Table 2: Characteristics of highest PGV earthquakes (see table 1 for all the earhquakes).